

## Continuous-wave spectroscopy of femtosecond carrier scattering in GaAs

G. Fasol, W. Hackenberg, and H. P. Hughes

*Cavendish Laboratory, Madingley Road, Cambridge CB3 0HE, United Kingdom*

K. Ploog and E. Bauser

*Max-Planck-Institut für Festkörperforschung, Heisenbergstrasse 1, D-7000 Stuttgart 80, West Germany*

H. Kano\*

*Toyota Central Research and Development Laboratories, Nagakute, Aichi 480-11, Japan*

(Received 7 August 1989)

We show that cw luminescence spectroscopy of the cascade of electrons in the conduction band of III-V compound semiconductors relaxing by LO-phonon emission yields information on the band structure, on electron-phonon, electron-electron, and intervalley scattering rates, and on impurity levels at higher-conduction-band minima in III-V compound semiconductors. The luminescence emitted by electrons recombining with holes on acceptors shows a series of up to nine very pronounced peaks directly measuring the steady-state distribution of electrons, while they cascade to the bottom of the conduction band in a few hundred femtoseconds. We determine the lifetime broadening by comparing the high-resolution cw hot-electron luminescence spectra with theoretical line shapes, calculated using a double- $\delta$ -function  $\mathbf{k}$ -space integration,  $16 \times 16$   $\mathbf{k} \cdot \mathbf{p}$  band structure, and transition-matrix elements in the dipole model. We determine an electron-LO-phonon scattering time of  $\tau_{LO} = (132 \pm 10)$  fs, and  $\Gamma \rightarrow L$  scattering times between  $\tau_{\Gamma \rightarrow L} = 150$  and 200 fs. We obtain  $D_{\Gamma \rightarrow L} = (9.5 \pm 1.5) \times 10^8$  eV/cm for the related deformation potential. We show how temperature-dependent scattering times, and electron-density-dependent scattering (i.e., electron-electron scattering) can be studied with the same method. Thus, we measure ultrafast processes by cw luminescence spectroscopy which are too fast or too weak for the sensitivity of present-day femtosecond spectroscopy. Unlike experiments using ultrashort laser pulses, the present method can study ultrafast (femtosecond) relaxation processes under low and high carrier concentration and with high spectral resolution.

### I. LUMINESCENCE FROM ELECTRONS IN THE LO-PHONON-EMISSION CASCADE

We present a method to study the femtosecond scattering processes of electrons in III-V compound semiconductors using continuous wave (cw) spectroscopy. Electron-electron scattering, electron-LO-phonon scattering, and  $\Gamma \rightarrow L$  scattering determine the behavior of fast transistors using these materials. Accurate values for the parameters determining femtosecond processes are very important for device modeling and understanding fundamental processes. Switching times of the fastest electronic and optical devices are reaching this time domain. New physical approaches are needed to describe ultrafast processes. There are still big discrepancies in the experimental determination of many fundamental scattering times, such as the technologically important  $\Gamma \rightarrow L$  scattering time in GaAs, which determines the saturation velocity in high-field transport. In the picosecond time domain, the most successful techniques have been pulsed laser techniques, often using a streak camera. In the femtosecond domain, pump and probe techniques are used. Pump and probe techniques using femtosecond laser pulses have severe limitations: their sensitivity is limited; the extremely high peak optical in-

tensities during the pulse duration severely perturb the sample; and due to the uncertainty principle the spectral width of ultrashort pulses is broad, restricting the spectral resolution of femtosecond spectroscopic experiments.

In the present work, we use an alternative approach. We use luminescence from the steady-state distribution of electrons in the conduction band of GaAs, which are excited by a continuous-wave laser. The principles of this technique and a typical spectrum are shown in Fig. 1. The luminescence is detected by standard cw photon counting. Thus we can study the processes of carrier relaxation and carrier scattering which take place on a 100-fs time scale. We benefit from the advantages of a cw technique: high sensitivity, high spectral resolution, and high dynamic range of the excitation density—we have recently studied the electronic relaxation in GaAs for carrier densities in the range  $10^{14}$ – $10^{17}$   $\text{cm}^{-3}$ . There is no difficulty in principle in extending this carrier density range in either direction.

Electrons excited high into the conduction band of GaAs relax predominantly by emission of LO phonons as long as the carrier density, the light intensity, and the temperature are low enough. Under these conditions the electrons relax by subsequent emission of LO phonons. As a result the steady-state distribution of electrons con-

sists of a cascade of peaks spaced approximately one LO-phonon energy apart. This series of peaks can be seen very clearly in appropriately designed luminescence experiments. The LO-phonon scattering time is  $(132 \pm 10)$  fs (as determined below from the line-shape analysis of the hot-electron luminescence spectra), while the free-electron to acceptor recombination time is approximately 10 ns. Thus it follows that the hot-electron luminescence is about  $10^{-5}$  times weaker than the band-gap-related luminescence.

We show in the present paper that the hot-electron luminescence spectra contain a wealth of information about carrier thermalization, intraband and interband scattering times, band structure, electron-phonon interaction, electron-electron scattering, and other ultrafast scattering processes. We present a series of experimental results demonstrating the power of this very sensitive cw method. We determine band-structure information of GaAs near point  $\Gamma$ , we study free-electron to the acceptor transitions, we determine the energy dependence of the LO-phonon scattering time, the energy dependence of the  $\Gamma \rightarrow L$  scattering time, the associated deformation potential, and we obtain information about a donor state at a higher conduction-band minimum. We will show how the present method can be used to obtain information on carrier-carrier scattering, and temperature-dependent scattering processes. There is a wealth of other information, which may be obtained in this way.

## II. RELEVANT PREVIOUS WORK ON HOT-ELECTRON LUMINESCENCE IN III-V COMPOUNDS

The main luminescence emission in GaAs is from band-gap-related processes (bound excitons, free-electron to acceptor transitions, etc.). On the high-energy side of the extremely strong band-gap-related luminescence peaks, the luminescence intensity decreases exponentially with increasing energy—sometimes over several decades in intensity. This exponential luminescence tail can be fitted by an exponential function and a temperature may be derived.<sup>1</sup> The temperature derived from such a fit is very commonly used to study the temperature of the electron gas as a function of laser pump density, time delay after a laser pulse, etc. A large amount of work has been published on this type of hot-electron luminescence, and despite some problems with the interpretation, it has become a common tool. The luminescence studied in the present paper is on the high-energy side of the exponential tail.

Luminescence spectra from the hot-electron cascade on the high-energy side of the exponential tail in GaAs was reported first by the Leningrad group<sup>2,3</sup> and has been recently reviewed in Ref. 4. The Leningrad group also calculated the polarization properties, and determined a value for the  $\Gamma \rightarrow L$  scattering time from depolarization measurements in a magnetic field. Recently the Leningrad group also reported data on the valence-band anisotropy from luminescence of the hot-electron cascade in InP.<sup>5</sup> We have previously reported experiments proving that the relevant luminescence transition is to an accep-

tor level,<sup>6</sup> we have shown how band-structure information can be obtained from hot-electron luminescence experiments,<sup>7,8</sup> we analyzed the hot-electron luminescence line shapes,<sup>8</sup> and we have shown that determining the intensities should enable the determination of scattering times such as the  $\Gamma \rightarrow L$  scattering time.<sup>7</sup> The experimental determination of the band structure with hot-electron luminescence is in fact analogous to energy-resolved photoemission experiments.<sup>9,10</sup> Using the same cw hot-electron luminescence technique, Ulbrich *et al.*<sup>11</sup> have recently determined experimental values for the  $\Gamma \rightarrow L$  scattering time from an analysis of the luminescence intensities. Several concepts important for the present work on electron relaxation are reviewed by Ulbrich.<sup>12</sup>

Olego *et al.*<sup>13</sup> reported luminescence from heavily  $p$ -type doped GaAs. In these samples there is a doping-induced band-gap narrowing of around 30–60 meV, which is absent in the present low-doped samples. Olego *et al.* found oscillatory luminescence spectra due to carriers returning from the  $L$  conduction-band valley into the point- $\Gamma$  valley.<sup>14</sup>

At this stage it should be stressed that “oscillatory photoconductivity” and “oscillatory luminescence excitation” are not related to the present work. Such oscillatory spectra have been a topic of intense study in the 1970s. For access to the vast literature on these effects see Refs. 15 and 16. Note that these effects arise from a dependence of the trapping cross section of defects as a function of the electron kinetic energy—they have a different physical origin than the spectra studied in the present work, and do not allow us to obtain the detailed band-structure information and determination of scattering rates discussed here.

In the present paper, we establish the recombination mechanism; we show how the present results are useful to determine band-structure data of GaAs near point  $\Gamma$ . We calculate the expected line shapes from a double- $\delta$ -function integration over all  $k$  space, taking the matrix elements into account in the dipole approximation. Comparing the calculated line shapes with the measured ones enables us to determine the LO-phonon emission time and the  $\Gamma \rightarrow L$  scattering time, and their dependence on the electron kinetic energy.

## III. EXPERIMENT

The experiments reported here were performed with several different spectrometers. We used 0.8-m and 1-m double-grating spectrometers (Spex, Jarrel Ash, and Jobin Yvon) combined with single-channel detection using cooled gallium arsenide photomultipliers and photon counting. In addition, experiments were performed using a DILOR 0.5-m triple monochromator combined with single-channel and multichannel light detection. We used argon-ion, krypton-ion, and dye lasers. For all experiments the samples were cooled in closed-cycle or flow cryostats to helium temperatures. The temperature was carefully monitored with a calibrated Ge resistor next to the sample. In addition, for most experiments the exponential luminescence tail on the high-energy side of the band-gap-related luminescence was used to monitor the

electronic temperature. The spectra were not corrected for the spectral response of the measurement systems.

The samples were Ge, Zn, Be, and C *p*-type doped GaAs samples grown by molecular-beam epitaxy (MBE) and by liquid-phase epitaxy (LPE) both at the Max-Planck-Institut in Stuttgart and at the Toyota Central Research and Development Laboratories. Most experiments are performed at 10 K, so that all acceptors are neutral.

#### IV. RECOMBINATION OF ELECTRONS IN THE LO-PHONON CASCADE WITH NEUTRAL ACCEPTORS

At the outset of this work it is necessary to explain the luminescence mechanism. Figure 1 demonstrates the hot-electron luminescence process giving rise to the oscillatory luminescence spectra studied here. A spectrally narrow continuous-wave laser shining onto a GaAs sample lifts electrons from the light-hole band, from the heavy-hole band, and from the split-off band into three narrow energy regions in the conduction band. The initial, unrelaxed distribution of electrons is broadened both by the anisotropy of the band structure and secondly by the very short lifetime of these states. The electrons excited by the laser relax by the emission of LO phonons. For polar semiconductors, electron scattering by LO phonons is the most important scattering mechanism as long as electron-electron and electron-hole scattering are negligible. As the LO-phonon energy near  $k=0$  shows little dispersion, the carriers proceed through a cascade of peaks, the spacing of which corresponds approximately to the LO-phonon energy. Depending on the laser energy, there are two, and for sufficiently high laser energies, three superimposed cascades, one each for electrons originating from the heavy-hole band, the light-hole band, and the split-off band, respectively. At higher excess energies, scattering processes to other conduction-band minima at points *X* and *L* compete with the LO-phonon-related cascade in the point- $\Gamma$  valley.

Figure 1 demonstrates this situation, and also it shows a typical hot-electron luminescence spectrum in the inset on a logarithmic scale. At the outset of this work we had to prove that the transition scheme shown in Fig. 1 is correct. This is particularly necessary, as similar but unrelated oscillatory structure in the luminescence excitation spectrum and in the photoconductivity as studied extensively in the 1970s does not monitor femtosecond processes but resonant capture rates by impurities. Therefore, we measured the hot-electron luminescence spectra of GaAs, *p*-type doped with Ge, Be, Zn, and C. Results are shown in Fig. 2 for a laser wavelength of 7525 Å and in Fig. 3 for 6764 Å. The spectra for each laser wavelength show a clear shift, which depends on the type of acceptor. The acceptor binding energies are 40.4 meV for Ge, 30.7 meV for Zn, 28.0 meV for Be, and 26.0 meV for C. Comparison of these shifts with the differences in acceptor binding energy proves that the recombination measured is between hot electrons and neutral acceptors.<sup>6</sup> Thus the hot-electron luminescence spectrum directly measures the steady-state distribution of electrons in the

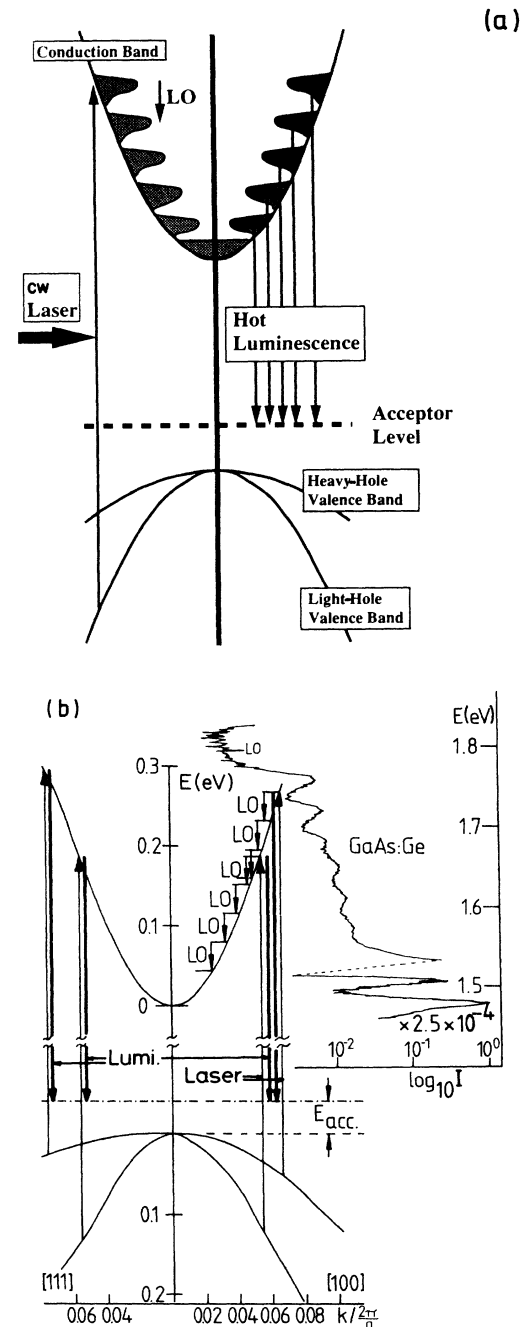


FIG. 1. (a) Schematic of cw spectroscopy of ultrafast processes in GaAs. The vertical arrow on the left shows excitation of electrons from the light-hole valence band to the conduction band by a cw dye laser. The steady-state distribution of electrons consists of a series of peaks, spaced by the LO-phonon energy. Individual electrons take only a few hundred femtoseconds to relax through this cascade. The luminescence transitions are indicated as vertical arrows. For clarity only processes involving the light-hole band are shown in (a). In the experiment, equivalent processes involving the heavy-hole band are superimposed. (b) This figure shows hot-electron luminescence near point  $\Gamma$  to scale. The steady-state distribution of electrons excited both from the heavy- and the light-hole bands are shown to scale. The inset on the right-hand side shows the corresponding luminescence spectrum on a logarithmic scale.

conduction band multiplied by the transition-matrix element between the conduction-band states and the acceptor state.

Figures 2 and 3 summarize several important results.

(1) The spacing of the peaks within each of the two series (for electrons from the heavy- and the light-hole bands) is around 38.5 meV, which is slightly larger than the LO-phonon energy of 36.4 meV.

(2) The separation of the first peak in each series with respect to the laser energy contains band-structure information. The horizontal bars show the expected contributions for electronic transitions taking place at the high-symmetry points  $X$ ,  $K$ , and  $L$  in  $k$  space.

(3) The luminescence peaks are broader than the width expected from the band structure. This broadening is due to lifetime broadening, provided electron-electron and electron-hole scattering, and other processes with small energy exchange, are excluded. Later in this paper we will determine scattering times from the broadening.

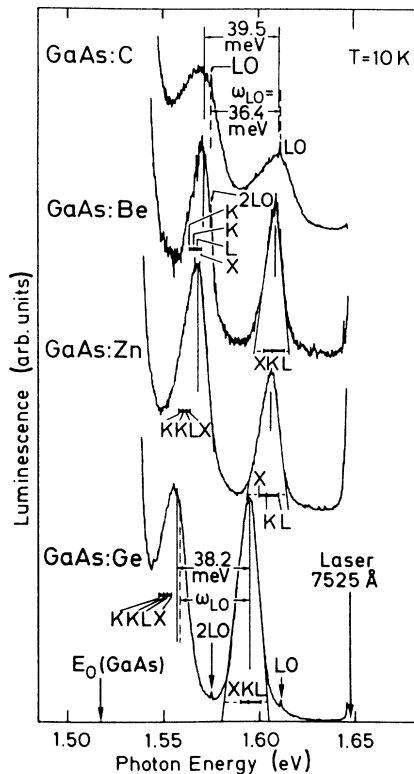


FIG. 2. Luminescence from the steady-state distribution of electrons in the conduction band of GaAs,  $p$ -type doped with C, Be, Zn, Ge. The shift between spectra corresponds exactly to the differences in acceptor binding energy proving that the transition is between the conduction band and the neutral acceptor. Note that the spacing is about 7% larger than the LO-phonon energy. The position of peaks is determined by the band structure. Contributions from the  $X$ ,  $K$ , and  $L$  directions in  $k$  space are indicated. Note that the measured spectrum is larger than the contributions expected from the band structure, reflecting lifetime broadening. Laser wavelength is 7525 Å.

## V. BAND-STRUCTURE INFORMATION FROM HOT-ELECTRON LUMINESCENCE SPECTRA

### A. Experiments

Figure 1 shows that the spacing between the first hot-electron luminescence peak and the laser corresponds to the initial kinetic energy of the hole plus the binding energy of the acceptor. Thus the position of the first hot-electron luminescence peak as a function of dye-laser energy contains band-structure information. This section will show how this information can be extracted and we will use our experiments to check the  $k \cdot p$  band-structure calculation in the first tenth of the Brillouin zone near point  $\Gamma$ .

Figure 4 shows a selection of measurements of hot-electron luminescence spectra in a Ge  $p$ -type doped GaAs sample for dye-laser energies ranging from 1.632 to 2.410 eV. The spectra show several types of peaks. There are series of peaks corresponding to the steady-state distribution of electrons relaxing by LO-phonon emission: the series of peaks just below the dye-laser energies corresponds to electrons originating from the heavy-hole (HH) band; a second series starts at somewhat lower energies and corresponds to electrons from the light-hole (LH) band. Both series of peaks move at different rates as the

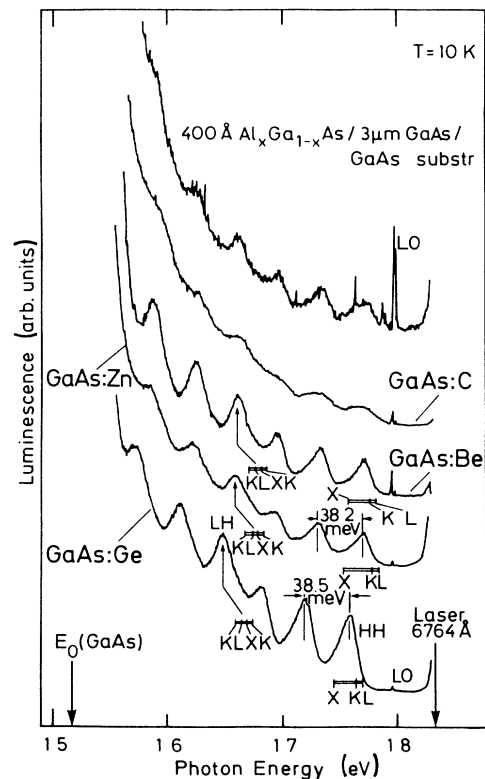


FIG. 3. Luminescence from the steady state of electrons relaxing by LO-phonon emission in GaAs  $p$ -type doped with C, Be, Zn, Ge. Analogous to Fig. 2, but for a laser wavelength of 6764 Å. Also measured is a sample covered with  $\text{Al}_x\text{Ga}_{1-x}\text{As}$ .

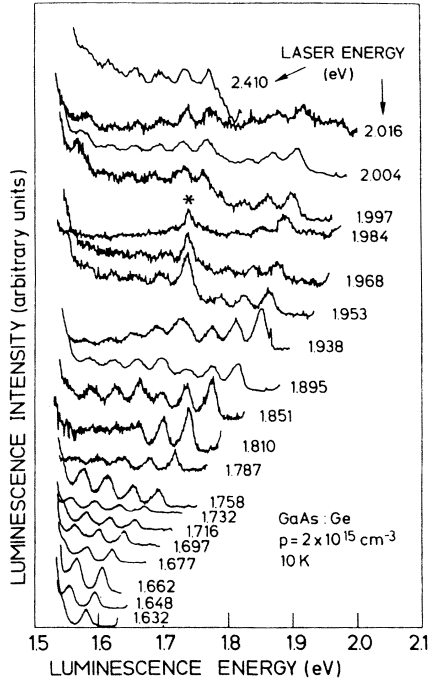


FIG. 4. Spectra of the steady-state distribution of electrons in the conduction band of GaAs for different dye-laser energies. The line shape of such spectra contains information on ultrafast carrier relaxation, and the position of the spectral peaks reflects the band structure.

dye-laser energy is varied, and there is a range of dye-laser energies (near 1.810 eV), where the peaks of the LH series fill the valleys of the HH series leading to a flat plateau in the spectra. Figure 5, for a dye-laser energy of 1.799 eV shows a spectrum, where the HH series and the LH series are well resolved. At still higher laser energies (above 1.953 eV) a hot-electron luminescence peak for

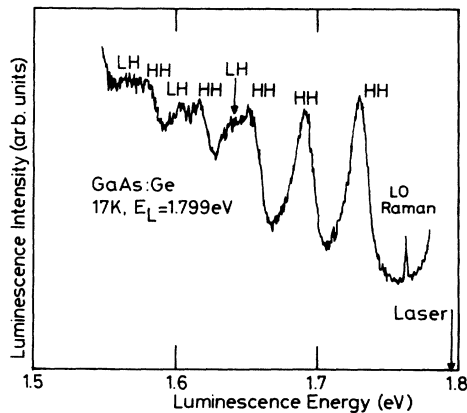


FIG. 5. Hot-electron luminescence spectrum for GaAs,  $p$ -type doped with a Ge spectrum. Laser wavelength is 6890 Å. This spectrum clearly shows the presence of one series of peaks corresponding to electrons from the heavy-hole band and a second series due to electrons from the light-hole band.

electrons from the split-off band appears close to the point where the exponential tail of the band-gap-related luminescence starts to rise. Further features of the spectra are a luminescence peak (shown with an asterisk) associated with a donor level at a higher conduction-band minimum, and luminescence from electrons returning after relaxation within the  $L$  conduction-band valley. These additional features will be discussed in later sections.

### B. Band structure and comparison with $16 \times 16$ $\mathbf{k} \cdot \mathbf{p}$ calculations

In the present section we extract band-structure information on GaAs from hot-electron luminescence spectra and we compare the results with the band structure calculated from a  $16 \times 16$   $\mathbf{k} \cdot \mathbf{p}$  Hamiltonian.

The  $\mathbf{k} \cdot \mathbf{p}$  technique is a perturbation technique to determine the dispersion of electron energy bands close to high-symmetry points. Many variants exist which differ mainly in the amount of terms in the perturbation expansion. Our present work is based on the  $14 \times 14$   $\mathbf{k} \cdot \mathbf{p}$  Hamiltonian given in Ref. 17. We have extended this Hamiltonian to include one more higher  $s$ -like ( $\Gamma'_1$ ) conduction band. In addition, we also include the spin-orbit coupling terms  $\Delta^-$  which were omitted in Ref. 17:

$$\langle (\frac{1}{2}, \frac{1}{2})_v | H_{s.o.} | (\frac{1}{2}, \frac{1}{2})_c \rangle = -\frac{2}{3}i\Delta^-, \quad (1a)$$

$$\langle (\frac{3}{2}, \frac{3}{2})_v | H_{s.o.} | (\frac{3}{2}, \frac{3}{2})_c \rangle = \frac{1}{3}i\Delta^-. \quad (1b)$$

Details of our  $16 \times 16$   $\mathbf{k} \cdot \mathbf{p}$  Hamiltonian, also used for the present work, are given in great detail in Ref. 18. Table I of Ref. 18 shows the values for the parameters we used in the calculation. In Ref. 18 we have also presented an investigation of the accuracy of the present  $\mathbf{k} \cdot \mathbf{p}$  calculation. We find good agreement with relativistic linear muffin-tin orbital (LMTO) calculations for at least the first tenth of the Brillouin zone, and for several bands far beyond.

One particular way of extracting band-structure information from the hot-electron luminescence spectra is shown in Fig. 6. The continuous lines in this figure show results from our  $\mathbf{k} \cdot \mathbf{p}$  band-structure calculations. Let us assume for the moment that the dispersion of the conduction band as a function of the wave vector  $\mathbf{k}$ , and the position of the acceptor level with respect to the conduction band, are well known. Then we can use the energy of the first hot-electron luminescence peak, which corresponds to the unrelaxed electrons, to determine the position along the  $\mathbf{k}$  axis where the excitation and the luminescence transition take place. At this point along the  $\mathbf{k}$  axis we then use the dye-laser energy, as shown in Fig. 6, to plot an experimental value for the valence band. Figure 6 shows such experimental points derived from around 50 measurements for the light-hole band, the heavy-hole band, and the split-off band. There is good agreement between the experimental points and the  $\mathbf{k} \cdot \mathbf{p}$  band structure. Nevertheless, it has to be kept in mind that the present experiments do not allow a directional resolution of the band structure.

In Fig. 7 the same data are analyzed in a different way.

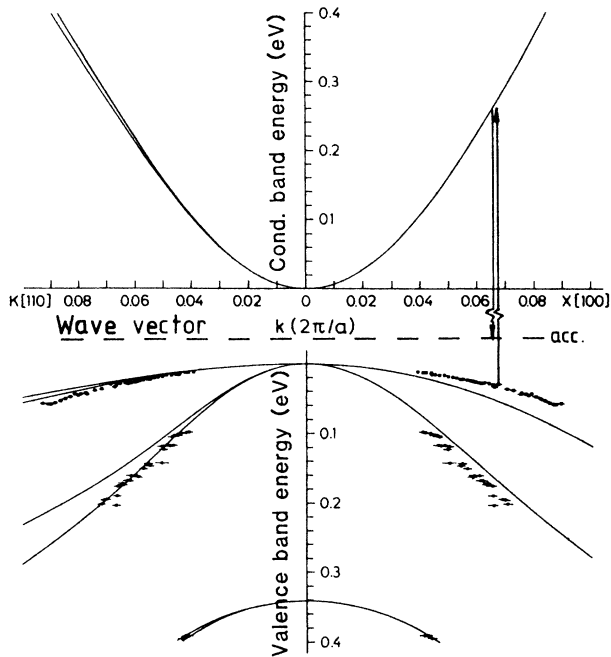


FIG. 6. This diagram shows that experimental values for the valence bands can be obtained from the positions of the hot-electron luminescence peaks, provided that the conduction band is known. There is no directional resolution.

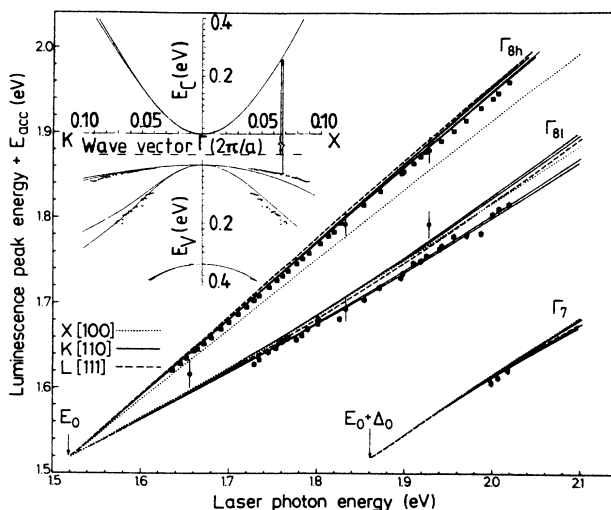


FIG. 7. Position of the hot-electron luminescence peaks (solid squares) as a function of dye-laser energy, in comparison to the positions expected in different directions in  $k$  space. Solid, dotted, and dashed lines show the results of a  $16 \times 16$   $k$ - $p$  calculation for the band structure of GaAs. This luminescence experiment is equivalent to energy-resolved photoemission results (solid dots) (Refs. 19 and 20). The inset on the left-hand side shows schematically the underlying luminescence process.  $E_v$  (eV) denotes the valence-band energy and  $E_c$  (eV) denotes the conduction-band energy.

We plot the energies of the hot-electron luminescence peaks (these energies are equivalent to the excess energies of the unrelaxed electrons plus the band-gap energy) as a function of the dye-laser energy. The experimental data (solid squares in Fig. 7) are compared with the results of our  $16 \times 16$   $k$ - $p$  calculation, which are shown for several directions of  $k$  space. There is generally very good agreement, keeping in mind that the experimental values give no information on the directional dependence of the band structure. Also shown in this figure are data from energy-resolved electron photoemission experiments<sup>19,20</sup> (solid circular points). These data have a somewhat larger vertical error bar, reflecting the comparatively lower energy resolution of photoemission experiments. Photoemission experiments, on the other hand, are possible to much higher energies, where the luminescence yield became too low for our measurement. The luminescence data agree very well with the results of photoemission experiments, confirming the accuracy of the  $k$ - $p$  band structure in this particular range.

Thus we have shown that hot-electron luminescence experiments are capable of delivering band-structure information in III-V compound semiconductors. They are equivalent to energy-resolved electron photoemission experiments, which have somewhat lower energy resolution than luminescence, but may be used over a larger energy range higher into the conduction band. Both techniques are equivalent, because they both measure the steady-state distribution of electrons in the conduction band. Hot-electron luminescence measures the steady-state distribution via transitions to the acceptor level, while photoemission measures transitions to the vacuum level, which is also independent of  $k$ .

## VI. CALCULATIONS OF THE cw HOT-ELECTRON LUMINESCENCE LINE SHAPES

### A. Double- $\delta$ -function integral

In the previous section we have shown how to extract band-structure information from the peak position of the hot-electron spectra alone. We will show that there is much more information contained in the line shape of hot-electron spectra: electron-electron scattering, LO-phonon scattering, and the  $\Gamma \rightarrow L$  intervalley scattering may all be studied. In order to extract such information it is necessary to calculate the theoretical shape of the electron distribution from the band structure.

We calculate the expected luminescence line shape from the first peak in the steady-state electron distribution. The electrons corresponding to the first peak have not yet undergone any relaxation by LO-phonon emission and as long as the temperature and the excitation power are low enough there will be no other scattering mechanism. Nevertheless, the spectra will be broadened by the limited lifetime due to LO-phonon emission, and by the  $\Gamma \rightarrow L$  and  $\Gamma \rightarrow X$  scattering mechanisms at higher laser energies. We determine the scattering times by convoluting the calculated line shapes with a broadening curve and comparing the broadened spectra with experiment.

In order to calculate the expected luminescence spectra

we use Fermi's golden rule. We perform a double- $\delta$ -function integral over the Brillouin zone describing the probability of both the excitation of the electron by absorption of a laser photon and the emission of a luminescence photon. According to Fermi's golden rule we calculate the luminescence line shape  $I(E_{\text{lum}})$  as

$$I(E_{\text{lum}}) \sim \int d^3k |M(\mathbf{k})|^2 \times \delta(E_{\text{cond}}(\mathbf{k}) - E_{\text{val}}(\mathbf{k}) - E_{\text{laser}}) \times \delta(E_{\text{cond}}(\mathbf{k}) + E_0 - E_{\text{acc}} - E_{\text{lum}}). \quad (2)$$

Here  $E_{\text{cond}}(\mathbf{k})$  is the  $\Gamma_6$  conduction-band energy dispersion and  $E_{\text{val}}(\mathbf{k})$  is the dispersion of the relevant valence band (heavy hole, light hole, or split-off). Both are measured from the minimum of the conduction band, i.e., conduction-band energies are positive while valence-band energies are negative.  $E_0$  is the band-gap energy ( $E_0 = 1.519$  eV for GaAs at 10 K).  $E_{\text{acc}}$  is the acceptor binding energy for the relevant acceptor (Ge, Be, C, or Zn in our case).  $M(\mathbf{k})$  is the product of the relevant transition-matrix elements: i.e., the product of the matrix element for excitation from the valence band to the conduction band and the matrix element for emission of the luminescence photon by recombination of the same electron with a hole on the neutral acceptor.  $M(\mathbf{k})$  depends on the polarization of the incoming light, on the polarization of the outgoing light and on the direction and magnitude of  $\mathbf{k}$ . Note that here the integral in Eq. (2) has to be performed over an appropriate part of the Brillouin zone, which is six times larger than the irreducible part, since the presence of the incoming and the outgoing light in the integral reduces the symmetry of the problem. The occupation probability factors  $f_{\text{val}}(k)$ ,  $1 - f_{\text{cond}}(k)$ ,  $f_{\text{acc}}(k)$ , etc., can all be neglected here, since they are all equal to unity here.

The calculated spectra depend considerably on the matrix elements  $M(\mathbf{k})$ . We calculate the polarization and  $\mathbf{k}$  dependence of  $M(\mathbf{k})$  in the dipole model as discussed in the following section. To calculate the shape of the luminescence spectra we integrate Eq. (2) over the whole Brillouin zone using a tetrahedron method due to Allen.<sup>21</sup> With this method the Brillouin zone is divided into small tetrahedra. The energies and weight functions are calculated for the corner points of each tetrahedron and linearly interpolated along the edges of the tetrahedron. The integral is then calculated analytically for each tetrahedron and summed over all tetrahedra.

### B. Transition-matrix elements in the dipole model

In this section we describe the calculation of the transition-matrix elements  $M(\mathbf{k})$  in Eq. (2).  $M(\mathbf{k})$  is the product of the matrix element for the excitation transition and the luminescence recombination transition. Because III-V compound semiconductors have no center of inversion, all bands are spin-split,<sup>18,22</sup> except in a few high-symmetry directions such as [100]. Therefore, when calculating the transition probability from the light-hole bands ( $\text{LH}_{+1/2}$  and  $\text{LH}_{-1/2}$ ) to the conduction bands ( $\text{CB}_{+1/2}$  and  $\text{CB}_{-1/2}$ ), for example, in general, contribu-

tions from four different transitions have to be summed:

$$\text{LH}_{+1/2} \rightarrow \text{CB}_{+1/2} \quad (\pi), \quad (3a)$$

$$\text{LH}_{+1/2} \rightarrow \text{CB}_{-1/2} \quad (\sigma_-), \quad (3b)$$

$$\text{LH}_{-1/2} \rightarrow \text{CB}_{+1/2} \quad (\sigma_+), \quad (3c)$$

$$\text{LH}_{-1/2} \rightarrow \text{CB}_{-1/2} \quad (\pi), \quad (3d)$$

where the arrows refer to the spin orientations with respect to the spin quantization axis.  $\pi$ ,  $\sigma_-$ , and  $\sigma_+$  refer to linearly oscillating, left-hand, and right-hand rotating dipoles associated with these transitions. The spin splitting is equivalent to the presence of a magnetic field acting on the electron spin. Note that both magnitude and orientation of the magnetic field depend on the orientation and magnitude of the electron wave vector  $\mathbf{k}$ . In the case of the heavy-hole bands the situation is slightly simpler, as in the present approximation only matrix elements for the following transitions exist:

$$\text{HH}_{+3/2} \rightarrow \text{CB}_{+1/2} \quad (\sigma_-), \quad (3e)$$

$$\text{HH}_{-3/2} \rightarrow \text{CB}_{-1/2} \quad (\sigma_+). \quad (3f)$$

We treat the emission and absorption of photons in the dipole model, i.e., we represent a particular transition by oscillating ( $\pi$ ) or by rotating dipoles ( $\sigma_-$  or  $\sigma_+$ ) to which the photon field couples via its electric field vector. The electric field vector is parallel to the polarization plane in the case of plane-polarized light [ $\pi$  in Eqs. (3)] and rotating in the case of circularly polarized light [ $\sigma_+$  and  $\sigma_-$  in Eqs. (3)]. Table I shows the dipoles associated with the various transitions: e.g.,  $\text{HH}_{+3/2} \rightarrow \text{CB}_{+1/2}$  corresponds to a rotating dipole. The rotational axis is parallel to  $\mathbf{k}$ .

To give an example, let us consider linearly polarized light with the electric field vector  $\mathcal{E}$  parallel to the unit vector  $\mathbf{e}$ . The matrix element  $\mathbf{m}$  of the optical transition  $\text{HH}_{+3/2} \rightarrow \text{CB}_{+1/2}$  is given by

$$\mathbf{m}^2 \sim [2^{-1/2}(\sin\theta)]^2 = \frac{1}{2} \left[ 1 - \left| \frac{\mathbf{k} \cdot \mathbf{e}}{|\mathbf{k}|} \right|^2 \right]. \quad (4)$$

$\mathbf{k}$  is the crystal wave vector of the electron and hole states (we neglect the wave vector of the photon),  $\mathbf{e}$  is the unit

TABLE I. Dipoles describing optical transitions between the spin-split valence bands and the spin-split conduction bands at point  $\Gamma$ .  $\kappa_{\parallel}$  is a unit vector parallel to the electron wave vector  $\mathbf{k}$ , while  $\kappa_{11}$  and  $\kappa_{12}$  are mutually perpendicular unit vectors perpendicular to  $\mathbf{k}$ . Thus,  $(\kappa_{11} + i\kappa_{12})$  describes a rotating dipole. HH stands for heavy-hole band, LH stands for light-hole band, SO for split-off, and CB for the lowest conduction band.

	$\text{CB}_{+1/2}$	$\text{CB}_{-1/2}$
$\text{HH}_{+3/2}$	$-(\kappa_{11} + i\kappa_{12})/\sqrt{2}$	0
$\text{HH}_{-3/2}$	0	$(\kappa_{11} - i\kappa_{12})/\sqrt{2}$
$\text{LH}_{+1/2}$	$\sqrt{2/3}\kappa_{\parallel}$	$-(\kappa_{11} + i\kappa_{12})/\sqrt{6}$
$\text{LH}_{-1/2}$	$(\kappa_{11} - i\kappa_{12})/\sqrt{6}$	$\sqrt{2/3}\kappa_{\parallel}$
$\text{SO}_{+1/2}$	$-\sqrt{1/3}\kappa_{\parallel}$	$-(\kappa_{11} + i\kappa_{12})/\sqrt{3}$
$\text{SO}_{-1/2}$	$-(\kappa_{11} - i\kappa_{12})/\sqrt{3}$	$-\sqrt{1/3}\kappa_{\parallel}$

TABLE II. Combined transition probabilities for laser excitation followed by hot-electron luminescence recombination with the acceptor. The acceptor is assumed to have a heavy-hole wave function.  $\mathbf{k}$  is the wave vector of the electron and hole states,  $\mathbf{e}_{\text{in}}$  and  $\mathbf{e}_{\text{out}}$  are unit vectors parallel to the  $\mathcal{E}$  field vectors of linearly polarized incoming and outgoing light, respectively,  $\boldsymbol{\eta}_{\text{in}}$  and  $\boldsymbol{\eta}_{\text{out}}$  are vectors perpendicular to the plane of rotation in the case of circularly polarized light.

	CB <sub>+1/2</sub>	CB <sub>-1/2</sub>
In, linear polarization; out, linear polarization		
HH <sub>+3/2</sub>	$\frac{1}{4} \left[ 1 - \left( \frac{\mathbf{k} \cdot \mathbf{e}_{\text{in}}}{ \mathbf{k} } \right)^2 \right] \left[ 1 - \left( \frac{\mathbf{k} \cdot \mathbf{e}_{\text{out}}}{ \mathbf{k} } \right)^2 \right]$	0
HH <sub>-3/2</sub>	0	$\frac{1}{4} \left[ 1 - \left( \frac{\mathbf{k} \cdot \mathbf{e}_{\text{in}}}{ \mathbf{k} } \right)^2 \right] \left[ 1 - \left( \frac{\mathbf{k} \cdot \mathbf{e}_{\text{out}}}{ \mathbf{k} } \right)^2 \right]$
LH <sub>+1/2</sub>	$\frac{1}{3} \left( \frac{\mathbf{k} \cdot \mathbf{e}_{\text{in}}}{ \mathbf{k} } \right)^2 \left[ 1 - \left( \frac{\mathbf{k} \cdot \mathbf{e}_{\text{out}}}{ \mathbf{k} } \right)^2 \right]$	$\frac{1}{12} \left[ 1 - \left( \frac{\mathbf{k} \cdot \mathbf{e}_{\text{in}}}{ \mathbf{k} } \right)^2 \right] \left[ 1 - \left( \frac{\mathbf{k} \cdot \mathbf{e}_{\text{out}}}{ \mathbf{k} } \right)^2 \right]$
LH <sub>-1/2</sub>	$\frac{1}{12} \left[ 1 - \left( \frac{\mathbf{k} \cdot \mathbf{e}_{\text{in}}}{ \mathbf{k} } \right)^2 \right] \left[ 1 - \left( \frac{\mathbf{k} \cdot \mathbf{e}_{\text{out}}}{ \mathbf{k} } \right)^2 \right]$	$\frac{1}{3} \left( \frac{\mathbf{k} \cdot \mathbf{e}_{\text{in}}}{ \mathbf{k} } \right)^2 \left[ 1 - \left( \frac{\mathbf{k} \cdot \mathbf{e}_{\text{out}}}{ \mathbf{k} } \right)^2 \right]$
In, linearly polarized; out, circularly polarized		
HH <sub>+3/2</sub>	$\frac{1}{4} \left[ 1 - \left( \frac{\mathbf{k} \cdot \mathbf{e}_{\text{in}}}{ \mathbf{k} } \right)^2 \right] \left[ 1 + \frac{\mathbf{k} \cdot \boldsymbol{\eta}_{\text{out}}}{ \mathbf{k} } \right]^2$	0
HH <sub>-3/2</sub>	0	$\frac{1}{4} \left[ 1 - \left( \frac{\mathbf{k} \cdot \mathbf{e}_{\text{in}}}{ \mathbf{k} } \right)^2 \right] \left[ 1 - \frac{\mathbf{k} \cdot \boldsymbol{\eta}_{\text{out}}}{ \mathbf{k} } \right]^2$
LH <sub>+1/2</sub>	$\frac{1}{3} \left( \frac{\mathbf{k} \cdot \mathbf{e}_{\text{in}}}{ \mathbf{k} } \right)^2 \left[ 1 + \frac{\mathbf{k} \cdot \boldsymbol{\eta}_{\text{out}}}{ \mathbf{k} } \right]^2$	$\frac{1}{12} \left[ 1 - \left( \frac{\mathbf{k} \cdot \mathbf{e}_{\text{in}}}{ \mathbf{k} } \right)^2 \right] \left[ 1 - \frac{\mathbf{k} \cdot \boldsymbol{\eta}_{\text{out}}}{ \mathbf{k} } \right]^2$
LH <sub>-1/2</sub>	$\frac{1}{12} \left[ 1 - \left( \frac{\mathbf{k} \cdot \mathbf{e}_{\text{in}}}{ \mathbf{k} } \right)^2 \right] \left[ 1 + \frac{\mathbf{k} \cdot \boldsymbol{\eta}_{\text{out}}}{ \mathbf{k} } \right]^2$	$\frac{1}{3} \left( \frac{\mathbf{k} \cdot \mathbf{e}_{\text{in}}}{ \mathbf{k} } \right)^2 \left[ 1 - \frac{\mathbf{k} \cdot \boldsymbol{\eta}_{\text{out}}}{ \mathbf{k} } \right]^2$
In, circular polarization; out, linear polarization		
HH <sub>+3/2</sub>	$\frac{1}{4} \left[ 1 + \frac{\mathbf{k} \cdot \boldsymbol{\eta}_{\text{in}}}{ \mathbf{k} } \right]^2 \left[ 1 - \left( \frac{\mathbf{k} \cdot \mathbf{e}_{\text{out}}}{ \mathbf{k} } \right)^2 \right]$	0
HH <sub>-3/2</sub>	0	$\frac{1}{4} \left[ 1 - \frac{\mathbf{k} \cdot \boldsymbol{\eta}_{\text{in}}}{ \mathbf{k} } \right]^2 \left[ 1 - \left( \frac{\mathbf{k} \cdot \mathbf{e}_{\text{out}}}{ \mathbf{k} } \right)^2 \right]$
LH <sub>+1/2</sub>	$\frac{1}{3} \left[ 1 - \left( \frac{\mathbf{k} \cdot \boldsymbol{\eta}_{\text{in}}}{ \mathbf{k} } \right)^2 \right] \left[ 1 - \left( \frac{\mathbf{k} \cdot \mathbf{e}_{\text{out}}}{ \mathbf{k} } \right)^2 \right]$	$\frac{1}{12} \left[ 1 + \frac{\mathbf{k} \cdot \boldsymbol{\eta}_{\text{in}}}{ \mathbf{k} } \right]^2 \left[ 1 - \left( \frac{\mathbf{k} \cdot \mathbf{e}_{\text{out}}}{ \mathbf{k} } \right)^2 \right]$
LH <sub>-1/2</sub>	$\frac{1}{12} \left[ 1 - \frac{\mathbf{k} \cdot \boldsymbol{\eta}_{\text{in}}}{ \mathbf{k} } \right]^2 \left[ 1 - \left( \frac{\mathbf{k} \cdot \mathbf{e}_{\text{out}}}{ \mathbf{k} } \right)^2 \right]$	$\frac{1}{3} \left[ 1 - \left( \frac{\mathbf{k} \cdot \boldsymbol{\eta}_{\text{in}}}{ \mathbf{k} } \right)^2 \right] \left[ 1 - \left( \frac{\mathbf{k} \cdot \mathbf{e}_{\text{out}}}{ \mathbf{k} } \right)^2 \right]$
In, circular polarization; out, circular polarization		
HH <sub>+3/2</sub>	$\frac{1}{4} \left[ 1 + \frac{\mathbf{k} \cdot \boldsymbol{\eta}_{\text{in}}}{ \mathbf{k} } \right]^2 \left[ 1 + \frac{\mathbf{k} \cdot \boldsymbol{\eta}_{\text{out}}}{ \mathbf{k} } \right]^2$	0
HH <sub>-3/2</sub>	0	$\frac{1}{4} \left[ 1 - \frac{\mathbf{k} \cdot \boldsymbol{\eta}_{\text{in}}}{ \mathbf{k} } \right]^2 \left[ 1 - \frac{\mathbf{k} \cdot \boldsymbol{\eta}_{\text{out}}}{ \mathbf{k} } \right]^2$
LH <sub>+1/2</sub>	$\frac{1}{3} \left[ 1 - \left( \frac{\mathbf{k} \cdot \boldsymbol{\eta}_{\text{in}}}{ \mathbf{k} } \right)^2 \right] \left[ 1 + \frac{\mathbf{k} \cdot \boldsymbol{\eta}_{\text{out}}}{ \mathbf{k} } \right]^2$	$\frac{1}{12} \left[ 1 + \frac{\mathbf{k} \cdot \boldsymbol{\eta}_{\text{in}}}{ \mathbf{k} } \right]^2 \left[ 1 - \frac{\mathbf{k} \cdot \boldsymbol{\eta}_{\text{out}}}{ \mathbf{k} } \right]^2$
LH <sub>-1/2</sub>	$\frac{1}{12} \left[ 1 - \frac{\mathbf{k} \cdot \boldsymbol{\eta}_{\text{in}}}{ \mathbf{k} } \right]^2 \left[ 1 + \frac{\mathbf{k} \cdot \boldsymbol{\eta}_{\text{out}}}{ \mathbf{k} } \right]^2$	$\frac{1}{3} \left[ 1 - \left( \frac{\mathbf{k} \cdot \boldsymbol{\eta}_{\text{in}}}{ \mathbf{k} } \right)^2 \right] \left[ 1 - \frac{\mathbf{k} \cdot \boldsymbol{\eta}_{\text{out}}}{ \mathbf{k} } \right]^2$



vector perpendicular to the plane in which the  $\mathcal{E}$  field of the circular polarized light associated with the  $\text{HH}_{+3/2} \rightarrow \text{CB}_{+1/2}$  transition rotates, and  $\theta$  is the angle between  $\mathbf{k}$  and  $\mathbf{e}$ . Thus plane-polarized light with  $\mathcal{E}$  perpendicular to the plane in which the dipole associated with a particular transition rotates will induce no transitions.

To calculate the hot-electron luminescence spectra we have to consider both the absorption process as well as the luminescence emission process. Thus  $|M(\mathbf{k})|^2$  in Eq. (2) is the product of the excitation probability and the luminescence emission probability. One of the greatest possible sources of error in the present calculation is the transition-matrix element to the acceptors and its  $\mathbf{k}$  dependence. Indeed, measurements of the hot-electron luminescence intensity as a function of dye-laser energy<sup>7,11</sup> may actually be used to determine the details of the acceptor wave function. In the present work, we simply assume that the acceptor wave function is predominantly formed from the heavy-hole wave function at the conduction-band maximum. We evaluate the matrix elements  $|M(\mathbf{k})|^2$  in the dipole model and the results are shown in Table II. Those values from Table II which are appropriate for the polarization conditions of the measurement are inserted into Eq. (2) to calculate the luminescence line shape.

It should be noted that the present dipole model is strictly only valid for transitions at  $\mathbf{k}=0$ . For  $\mathbf{k} \neq 0$ , heavy- and light-hole bands mix. The present calculation can easily be extended to treat the transition-matrix elements in the  $\mathbf{k} \cdot \mathbf{p}$  approximation, since the optical-matrix elements and the  $\mathbf{k} \cdot \mathbf{p}$  matrix elements are identical.

### C. Comparison of the calculated and measured hot-electron luminescence shapes

Detailed comparison of the calculated hot-electron luminescence line shape and measurement for a  $p$ -type GaAs:Ge sample are shown in Fig. 8. The solid line is

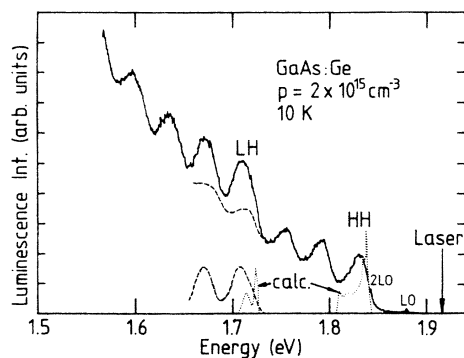


FIG. 8. The solid line shows the experimental hot-electron luminescence spectrum for GaAs:Ge and a laser wavelength of 6471 Å. The dotted lines show the unbroadened (neglecting lifetime broadening) calculated spectra for the heavy-hole and the light-hole band. The calculations use a  $16 \times 16$   $\mathbf{k} \cdot \mathbf{p}$  matrix for the electronic band structure, a double- $\delta$ -function  $\mathbf{k}$ -space integral and transition-matrix elements in the dipole model (see text).

the measured hot-electron luminescence spectrum for the laser wavelength 6471 Å, displaying one series of peaks for electrons excited from the heavy-hole band. Below 1.73 eV this series is extrapolated to lower energies. Superimposed onto this first series is the second series for electrons from the light-hole band. Subtracting the extrapolated HH series (dashed line) we determine the contribution from the LH series alone; we show the resulting LH hot-electron luminescence as a dashed line below 1.73 eV.

The dotted lines are the corresponding calculated hot-electron luminescence line shapes for the first electron peak, where the excited electrons have not undergone any relaxation process. The hot-electron luminescence band for electrons excited from the HH valence band appears between around 1.85 and 1.81 eV for this particular dye-laser energy. There is a strong peak near 1.84 eV followed by a shoulder, which has two weaker peaks near 1.82 eV. Comparison with the horizontal bars which indicate the contributions from different regions in  $\mathbf{k}$  space in Fig. 3 and with the lines shown in Fig. 7 shows that the first strong peak near 1.84 eV corresponds to electrons from regions of  $\mathbf{k}$  space such as the directions pointing towards points  $K$  and  $L$ . The peak at lower energies near 1.82 eV corresponds to transitions near the  $\Delta$  directions. The luminescence in this shoulder is weaker, as the density of states is lower near  $X$  (where the effective mass is lower) than near points  $K$  and  $L$ . The dotted peak between 1.73 and 1.71 eV displays the calculated hot-electron luminescence spectrum for electrons from the light-hole band. There are two peaks separated by 10 meV. Inspection of Fig. 7 and its inset show that this splitting observed in the LH peak is due to the spin splitting.<sup>18,22</sup> In the experimental spectra the effect of spin splitting is obscured by strong lifetime broadening.

Figure 9 shows measurements and calculations of the first luminescence peak, which results from electrons which have not yet undergone any emission of LO phonons. The measured luminescence bandwidths are in every case larger than the calculated widths. There may be several physical origins for broadening of the experi-

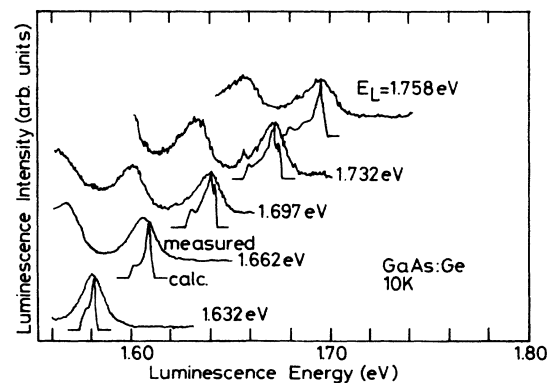


FIG. 9. Line-shape calculations analogous to Fig. 8 for several different laser energies. The experimental width is larger than the calculated width due to lifetime broadening.

mental line shape with respect to our raw (i.e., not lifetime broadened) calculation.

*Lifetime broadening* of the electron energy levels themselves, according to Heisenberg's uncertainty relationship  $\Delta E \Delta t \approx \hbar/2\pi$ . (To indicate the range: A scattering time of  $\Delta t = \tau = 150$  fs corresponds to a linewidth of  $\Delta E \approx 4.4$  meV, while a scattering time of  $\Delta t = \tau = 200$  fs yields a lifetime broadening of 3.3 meV.)

*Fast scattering mechanisms with small energy exchange.* If such processes are as fast as LO-phonon scattering they may yield a broadening of the distribution of electrons sampled by the luminescence measurement. Candidates are electron-electron scattering, electron-hole scattering, and acoustic-phonon scattering.

*Broadening of the acceptor ground state.* This will be important when the acceptor concentration is high enough to yield an impurity band. In our samples the doping concentration is always sufficiently low to avoid broadening due the acceptor wave-function overlap. We have observed a broadening of the hot-electron luminescence bands for higher acceptor concentrations.

We will show in later sections that precise analysis of the calculated and measured line shapes allows (a) an accurate determination of the LO-phonon scattering time as a function of the electron kinetic energy and (b) a determination of the  $\Gamma \rightarrow L$  (and analogously also the  $\Gamma \rightarrow X$  scattering time, although this is not shown in the present paper). (c) Measurements as a function of carrier density allow the analysis of electron-electron and electron-hole scattering.

## VII. DETERMINATION OF SCATTERING TIMES

cw hot-electron luminescence are ideally suited to determine details of ultrafast recombination and scattering processes. Scattering rates may be deduced in several ways from cw hot-electron luminescence experiments.

Depolarization of the cw hot-electron luminescence in a magnetic field. This technique was used by the Lenigrad group<sup>2</sup> to determine the  $\Gamma \rightarrow L$  scattering time.

Measurement of the cw hot-electron luminescence intensity as a function of the dye-laser energy and therefore as a function of electron kinetic energy. This technique was proposed by Fasol and Hughes<sup>7</sup> and was thoroughly studied by Ulbrich *et al.*<sup>11</sup> to determine the  $\Gamma \rightarrow L$  and the  $\Gamma \rightarrow X$  scattering times. The main limitation of this technique is the uncertainty in the present-day knowledge of the precise composition of the acceptor wave function and the matrix elements from the conduction band to the acceptors.

In the following sections (Secs. VII B and VII C of the present paper) we introduce an alternative method, which greatly reduces the uncertainty in the determination of scattering times from the lack of precise knowledge of the wave functions and matrix elements associated with the different acceptors in question. For this technique, we calculate the expected luminescence spectra using a  $\mathbf{k}$ - $\mathbf{p}$  band-structure calculation, and we determine the lifetime broadening by comparison of the measured and calculated luminescence shapes. For this determination only the relative variation of the acceptor matrix elements over a

very narrow energy range need be known, and not over the whole energy range of the full hot-electron luminescence spectrum.

In the following sections we first discuss the ratio of intensity of the hot-electron luminescence spectra compared to the band-gap luminescence, since it reflects the ratio of the LO-phonon scattering time to the recombination time for band-gap-related luminescence. Then we introduce the techniques for the lifetime determination from comparison of calculated and measured spectra.

Note that in order to deduce scattering times it is crucial to deconvolute the contributions from different scattering processes properly. In particular, acoustic-phonon, electron-electron, and electron-hole scattering will also contribute to the broadening of the distribution via exchange of small energy amounts. All experiments in the following sections are done under conditions designed to exclude contributions from acoustic-phonon, electron-electron, and electron-hole scattering.

### A. Ratio of band-gap related luminescence and hot-electron luminescence

Figure 10(a) shows the emission spectrum of a sample of GaAs:Ge ( $p \approx 4.9 \times 10^{15} \text{ cm}^{-3}$ ), while Fig. 10(b) is for GaAs:Ge with a slightly lower doping concentration ( $p \approx 2.1 \times 10^{15} \text{ cm}^{-3}$ ). The luminescence spectra are displayed logarithmically over 7 decades. The large dynamic range of these measurements was achieved by a long integration time in a single-photon counting mode and by the use of gray filters attenuating the band-gap-related emission. Figure 10 displays two band-gap-related luminescence lines—one line due to excitons bound to the acceptors and a much stronger second line due to free-electron to acceptor emission. If we neglect nonradiative processes, the ratio between the integral count rate for the band-gap-related luminescence  $I_{\text{gap}}$  and the first hot-electron peak  $I_{\text{cond} \rightarrow \text{acc}}$  is expected to be equal to the ratio of the conduction-band to acceptor transition time  $\tau_{\text{cond} \rightarrow \text{acc}}(\mathbf{k})$  and the LO-phonon scattering time  $\tau_{\text{LO}}$ . Therefore we expect

$$\begin{aligned} I_{\text{gap}} / I_{\text{cond} \rightarrow \text{acc}} &\approx \tau_{\text{cond} \rightarrow \text{acc}}(\mathbf{k}) / \tau_{\text{LO}} \\ &\approx (10 \text{ ns}) / (135 \text{ fs}) \approx 7 \times 10^4. \end{aligned} \quad (5)$$

This estimation is to be compared with the measurements of Fig. 10—note that Eq. (5) refers to the integrated intensity as opposed to the peak values. The comparison suggests that  $\tau_{\text{cond} \rightarrow \text{acc}}$  is actually longer than 10 ns.

### B. The LO-phonon scattering time

Figure 9 has shown the comparison of typical measured hot-electron spectra compared with spectra calculated without taking any lifetime or scattering effects into account. The measured spectra are considerably broader than the calculated shapes. The dominating scattering events are LO-phonon scattering below the threshold for scattering to the  $L$  conduction-band valley. Above this threshold, both LO-phonon scattering and scattering into the  $L$  valley contribute. As the temperature is low ( $T = 10$  K) and the photoinduced carrier density is low (below  $10^{15} \text{ cm}^{-3}$ ), acoustic-phonon, electron-electron,

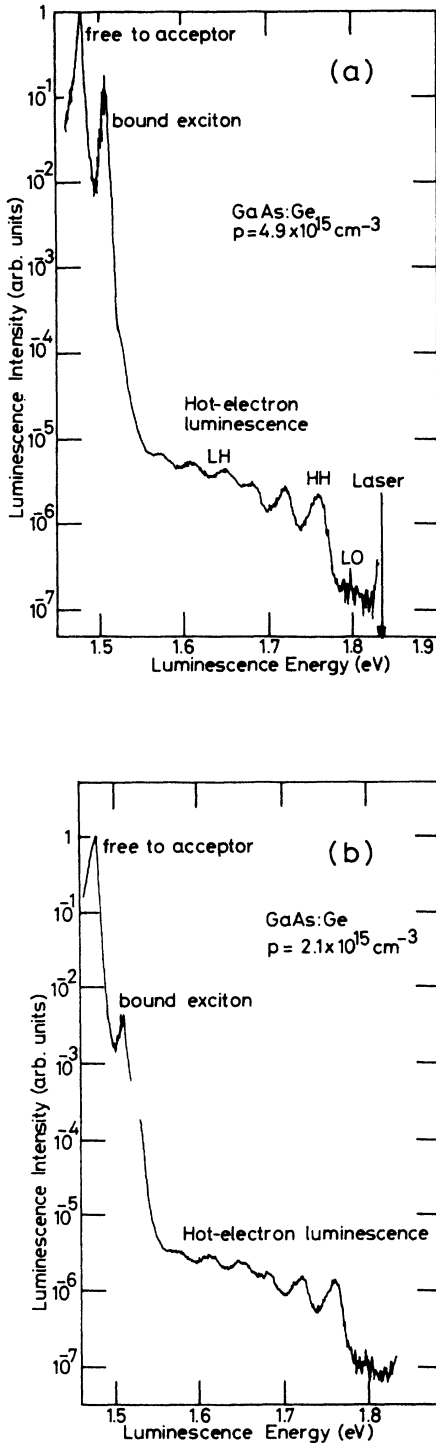


FIG. 10. (a) Hot-electron luminescence for GaAs *p*-type doped with Ge (carrier concentration at 77 K is  $4.9 \times 10^{15} \text{ cm}^{-3}$ ). The luminescence is shown logarithmically over 7 decades. The large dynamic range was achieved due to long integration time and the use of neutral density filters. The intensity ratio of band-gap-related luminescence and hot-electron cascade is related to the ratios of electron-LO-phonon scattering time (determined here as 132 fs) and band-gap relaxation time (approximately 1–10 ns). (b) Hot-electron luminescence spectrum as in (a) but for a Ge-doped GaAs sample with a lower carrier concentration ( $2.1 \times 10^{15} \text{ cm}^{-3}$  at  $T = 77 \text{ K}$ ).

and electron-hole scattering have negligible influence. We have checked this assumption by investigating the spectra as a function of induced carrier density. We found that considerably higher induced carrier densities are necessary to observe broadening effects due to carrier-carrier scattering. Figure 11 shows the comparison of a measurement (left-hand side) of the first luminescence peak due to electrons from the heavy-hole band, which have not yet undergone any LO-phonon emission, with an unbroadened and a broadened calculated spectrum for the same laser energy and polarization conditions. The calculations were done using a  $16 \times 16$   $\mathbf{k} \cdot \mathbf{p}$  matrix for the band structure of GaAs and integrating the double- $\delta$ -function integral describing the optical transitions over an appropriate part of  $\mathbf{k}$  space as described above in Sec. VI. The asymmetric shape of the calculated spectrum reflects the directional anisotropy of the valence-band dispersion. Effects of the spin splitting can also be seen in the unbroadened spectrum. We determined the lifetime by optimizing the theoretical fit to the experimental spectral shape. An example of such a fit is also shown on the right-hand side of Fig. 11.

By fitting a large number of spectra measured with different dye-laser energies we determine the electron lifetimes as a function of electron kinetic energy. The dependence of the total lifetimes on electron kinetic energy is shown in Fig. 12(a). The lifetimes are approximately constant up to an electron kinetic energy of around 300 meV. Above 300 meV, the lifetimes start to decrease with increasing electron kinetic energy. We attribute the decreased total lifetime above 300 meV to the onset of  $\Gamma \rightarrow L$  scattering.

We can neglect acoustic-phonon scattering at the present low temperatures. The present experiments are performed with a laser-induced carrier concentration of around  $10^{14} \text{ cm}^{-3}$ . Therefore, electron-electron and electron-hole scattering are also unimportant. Figure 12(a) shows that the scattering time is constant to within our error for electron kinetic energies between 100 and 300 meV. We determine the value  $\tau_{\text{LO}} = 132 \pm 10 \text{ fs}$ . This value lies well within the range of 100 to 200 fs reported

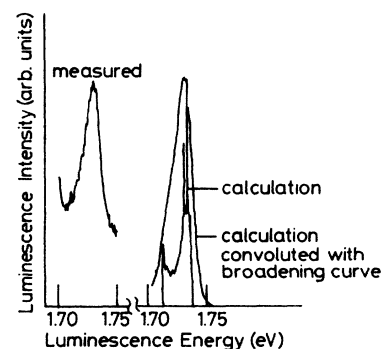


FIG. 11. Left-hand curve: measured cw hot-electron luminescence peak; right-hand curve, unbroadened calculated spectrum, and calculated lifetime-broadened spectrum. The lifetime-broadening parameter was determined as a fit parameter, to yield the best agreement with the experimental curve.

in recent years. It is important to keep in mind that in our case the carrier density is below  $10^{15} \text{ cm}^{-3}$ . For comparison, Kash *et al.*<sup>23</sup> have recently deduced a value of  $\tau_{\text{LO}} = 165 \text{ fs}$  from pump and probe Raman experiments at

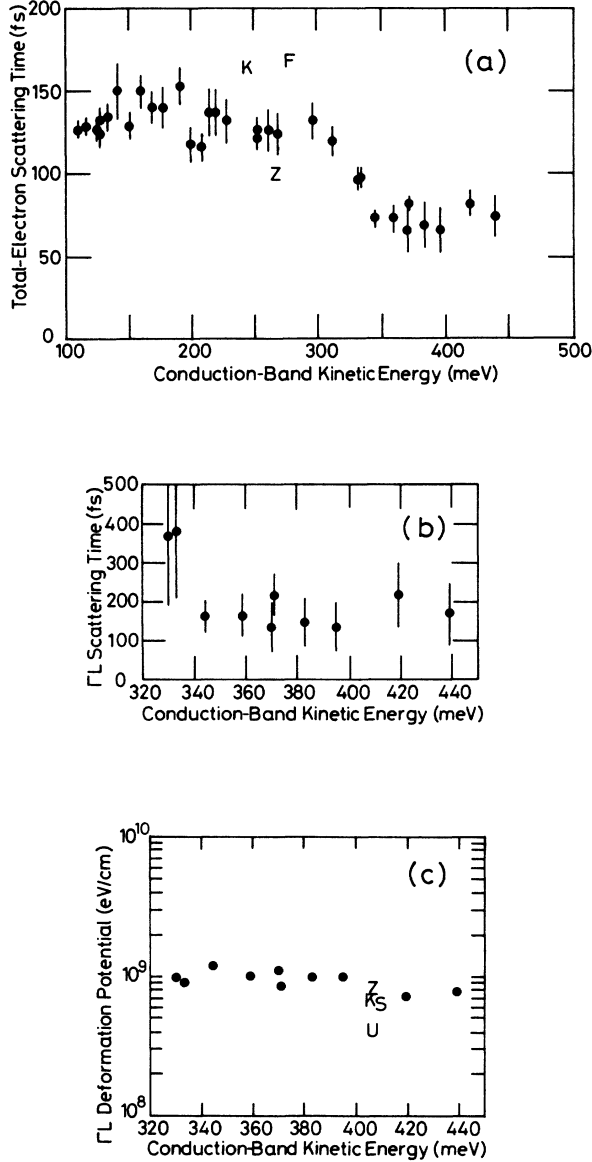


FIG. 12. (a) Total lifetime for electrons in the conduction band of GaAs determined by achieving the best fit between lifetime-broadened calculated spectra and measured cw hot-electron luminescence spectra. Symbols K, F, and Z indicate results of Kash *et al.* (Ref. 23), Fawcett *et al.* (Ref. 37), and Zakharchenya *et al.* (Ref. 2). (b)  $\Gamma \rightarrow L$  scattering time determined by deconvoluting the LO-phonon scattering and the  $\Gamma \rightarrow L$  scattering contributions. This figure represents our experimental results for the  $\Gamma \rightarrow L$  scattering time. (c)  $\Gamma \rightarrow L$  deformation potential determined from the scattering times shown in (b). Symbols Z, K, S, and U indicate results by Zakharchenya *et al.* (Ref. 2), Kash *et al.* (Ref. 38), Shah *et al.* (Ref. 25), and Ulbrich *et al.* (Ref. 11).

room temperature. From depolarization experiments of the hot-electron luminescence Zakharchenya *et al.*<sup>2</sup> find  $\tau_{\text{LO}} = 100 \pm 5 \text{ fs}$  at an electron kinetic energy of 260 meV. Levi *et al.*<sup>24</sup> find  $\tau_{\text{tot}} = 100 \text{ fs}$  from measurements in hot-electron transistors, which constitutes a lower limit to the LO-phonon scattering time, as other scattering effects are also expected to contribute. Thus our experimental determination of the kinetic energy dependence of the LO-phonon scattering time is consistent with recent available experimental data—a comparison is shown in Table III. Note that our data are for low carrier concentration.

### C. The $\Gamma \rightarrow L$ scattering time

Figure 12(a) showed that the total electron lifetime decreases when the electron kinetic energy increases above 300 meV, where  $\Gamma \rightarrow L$  scattering sets in. We assume that  $\tau_{\text{LO}}$  is constant within our required accuracy for energies higher than 300 meV, which is an assumption well supported by calculations. Using

$$1/\tau_{\text{tot}} = 1/\tau_{\text{LO}} + 1/\tau_{\Gamma \rightarrow L}, \quad (6)$$

we deduce the kinetic energy dependence of the  $\Gamma \rightarrow L$  scattering time  $\tau_{\Gamma \rightarrow L}$ . The results are shown in Fig. 12(b).

We calculate the corresponding deformation potential for  $\Gamma \rightarrow L$  scattering from the following relationship:<sup>26</sup>

$$1/\tau_{\Gamma L} = (4D_{\Gamma \rightarrow L}^2 m_L^{3/2} / 2^{1/2} \pi \hbar^3 \rho \omega_{\text{ZB}}) \times [E - \hbar \omega_{\text{ZB}} - (E_L - E_{\Gamma})]^{1/2}, \quad (7)$$

where  $m_L = (m_L^x m_L^y m_L^z)^{1/3} = 0.22 m_0$  is the directionally weighted effective mass near the  $L$  conduction-band valley,  $\rho = 5.37 \text{ g cm}^{-3}$  is the density of GaAs, and  $\hbar \omega_{\text{ZB}} = 29.6 \text{ meV}$  is the average energy of the [111] zone-boundary (ZB) phonons responsible for the intervalley transfer.  $(E_L - E_{\Gamma})$  is the energy of the bottom of the  $L$  valleys measured from the conduction-band minimum at point  $\Gamma$ .

Figure 12(c) shows the deformation potential  $D_{\Gamma \rightarrow L}$  for  $\Gamma \rightarrow L$  scattering determined from the data in Fig. 12(b) and using Eq. (7). We find that the deformation potential is virtually independent of the electron kinetic energy within our experimental accuracy. We find  $D_{\Gamma \rightarrow L} = (9.5 \pm 1.6) \times 10^8 \text{ eV/cm}$ . Table IV shows that the discrepancies between the values determined by different authors for  $D_{\Gamma \rightarrow L}$  are large. Shah *et al.*<sup>25</sup> find  $D_{\Gamma \rightarrow L} = (6.5 \pm 1.5) \times 10^8 \text{ eV/cm}$ . Collins and Yu<sup>26</sup> find  $D_{\Gamma \rightarrow L} = 1.5 \times 10^8 \text{ eV/cm}$ , but it can be shown that the hot-phonon population, on which the determination of Collins and Yu relies, is relatively insensitive to  $D_{\Gamma \rightarrow L}$ . Ulbrich *et al.*<sup>11</sup> find  $D_{\Gamma \rightarrow L} = (4.0 \pm 0.5) \times 10^8 \text{ eV/cm}$  from intensity measurements of the cw hot-electron luminescence measurements. The experimental method is comparable to the one used here, except that these authors use the dependence of the luminescence intensity as a function of electron kinetic energy, while we use the line shape as compared to the calculated line shapes. Ul-

TABLE III. Scattering times of electrons in the conduction band of GaAs by LO phonons.

$\tau_{LO}$	Reference	Method	Comments
132±10 fs	Present work	cw luminescence spectroscopy	$T = 10$ K
> 300 fs	Conwell <i>et al.</i> <sup>a</sup>	Calculation	
170 fs	Fawcett <i>et al.</i> <sup>b</sup>	Calculation	
100±5 fs	Zakharchenya <i>et al.</i> <sup>c</sup>	Magnetic depolarization of hot-electron luminescence	
165 fs	Kash <i>et al.</i> <sup>d</sup>	Time-resolved Raman	Room temperature
> 100 fs	Levi <i>et al.</i> <sup>e</sup>	Hot-carrier injection	

<sup>a</sup>E. Conwell and M. Vassell, Phys. Rev. **166**, 797 (1968).

<sup>b</sup>Reference 37.

<sup>c</sup>Reference 2.

<sup>d</sup>Reference 23.

<sup>e</sup>Reference 24.

Ulbrich *et al.*<sup>11</sup> use an LO-phonon scattering time of 180 fs, which is somewhat longer than in our present results. Note that the interpretation of Ulbrich *et al.* relies on the knowledge of the acceptor wave function over a large region of  $\mathbf{k}$ . In our interpretation, using line-shape calculations, this uncertainty is removed to a large extent. A comparison of our data with these and other determinations are shown in Table IV.

#### D. A method to study other scattering mechanisms

Since we are measuring the *total* broadening, we are able to determine effects of other scattering effects in addition to LO-phonon scattering and scattering to the  $L$  conduction-band valley. This is done by deconvoluting the various scattering mechanisms such as those de-

scribed above. The effect of electron-electron scattering is determined by measuring the hot-electron luminescence spectra as a function of carrier concentration. We have recently done such experiments, and they will be published separately. Additional scattering mechanisms setting in at higher temperatures can be analyzed. The dependence of the  $\Gamma \rightarrow L$  scattering on temperature and carrier concentration can also be measured in a straightforward way.

#### VIII. SPACING OF HOT-ELECTRON PEAKS

We have shown in Figs. 2 and 3 that the spacings of the luminescence peaks are about 7% larger than the LO-phonon energy at  $\mathbf{k}=0$ , which is 36.4 meV. This ex-

TABLE IV. Values for the deformation potential  $D_{\Gamma \rightarrow L}$  for scattering of electrons from the  $\Gamma$  to the  $L$  conduction-band valley.

$D_{\Gamma \rightarrow L}$ ( $10^8$ eV/cm)	Reference	Method	Comments
9.5±1.5	Present work	cw luminescence spectroscopy	$T = 10$ K
6.5±0.5	Shah <i>et al.</i> <sup>a</sup>	Time-resolved femtosecond spectroscopy	
4.0±0.5	Ulbrich <i>et al.</i> <sup>b</sup>	cw luminescence spectroscopy	
7.1±1.2	K. Kash <i>et al.</i> <sup>c</sup>	Nonlinear susceptibility measurements	
8.0±1.5	Zakharchenya <i>et al.</i> <sup>d</sup>	Magnetic depolarization of hot-electron luminescence	
1.5	Collins <i>et al.</i> <sup>e</sup>	Raman: determination of nonequilibrium phonon population	
10.0	Littlejohn <i>et al.</i> <sup>f</sup>	Velocity vs field calculation	

<sup>a</sup>Reference 25.

<sup>b</sup>Reference 11.

<sup>c</sup>Reference 38.

<sup>d</sup>Reference 2.

<sup>e</sup>Reference 26.

<sup>f</sup>M. Littlejohn, J. Hauser, and T. Glisson, J. Appl. Phys. **48**, 4587 (1977).

perimental result is shown in greater detail in Fig. 13. We show the energy shift between peaks 1 and 2 (crosses) and, secondly, also the shift between peaks 2 and 3 (solid dots) in the hot-electron spectra. These results are shown for a variety of samples and a variety of dye-laser energies. Figure 13 clearly shows that the peak separation is consistently larger than the LO-phonon energy. Figures 2 and 3 show that the peak spacing is larger than the LO-phonon energy for samples doped with any of the four acceptor species we investigated (C, Be, Ge, and Zn).

We have considered a variety of possible explanations for this experimental result. The most likely explanation is due to Ulbrich.<sup>27</sup> In his model, the energy shift is due to the change in the mutual Coulomb energy as the electron and the hole move apart between the time of generation and the instant of luminescence emission. Other possibilities that we have considered include a renormalization of the phonon energy in the vicinity of the acceptor impurity.<sup>28,29</sup> This explanation is unlikely, as the renormalization would be expected to change sign depending on whether the phonon energy is larger or smaller than the acceptor binding energy. Thus a decrease of the phonon energy would be expected for Ge, since the Ge acceptor binding energy<sup>30</sup> ( $40.4 \pm 1.0$  meV) is larger than the LO-phonon energy (36.4 meV). An increase would be expected for the other acceptors investigated here, as their binding energy is smaller than 36.4 meV. Our experiments contradict this prediction. Another possibility would be the polaron coupling, i.e., renormalization of phonon and excitonic energies due to their mutual interaction via the polarization fields. An argument against this explanation is the very small polaron correction to the effective mass in GaAs.

The previous discussion promises that the spacing of the hot-electron luminescence peaks within the LO-phonon cascades may reveal details of the carrier diffusion on an ultrafast time scale.

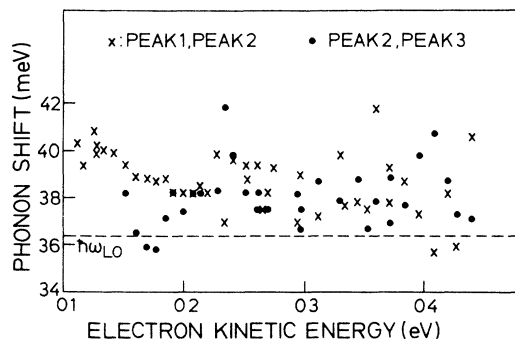


FIG. 13. The spacing of hot-electron peaks is about 7% larger than the LO-phonon energy. This figure demonstrates the spacing of a large number of spectra for different laser energies and different samples. Crosses indicate spacings between the first and second peaks, while dots indicate spacings between the second and third peaks.

## IX. TEMPERATURE DEPENDENCE

We studied the influence of temperature on the hot-electron cascade luminescence. Figure 14 shows spectra at  $T=10$  and 80 K. The temperatures were measured with a calibrated Ge resistor in contact with the cold finger of the helium-flow cryostat. The temperature was kept at a constant value by a temperature controller, and the simultaneous use of a He-flow regulator and a heater. Figure 14(a) shows results for  $p$ -type GaAs:Ge ( $n_p \approx 1.7 \times 10^{16} \text{ cm}^{-3}$  at  $T=77$  K) and Fig. 14(b) for  $p$ -type GaAs:Be ( $n_p \approx 2.5 \times 10^{16} \text{ cm}^{-3}$  at  $T=77$  K). Both Figs. 14(a) and 14(b) show that the global features of the luminescence from the LO-phonon hot-electron cascade, such as the integrated intensity and the position of the peaks, stay unaffected by temperature, but the individual peaks broaden substantially. At low energies, below 1.6 eV, the luminescence rises stronger as the energy decreases for the higher temperature, reflecting the well-known temperature dependence of the exponential tail of the band-gap-related luminescence. The substantial

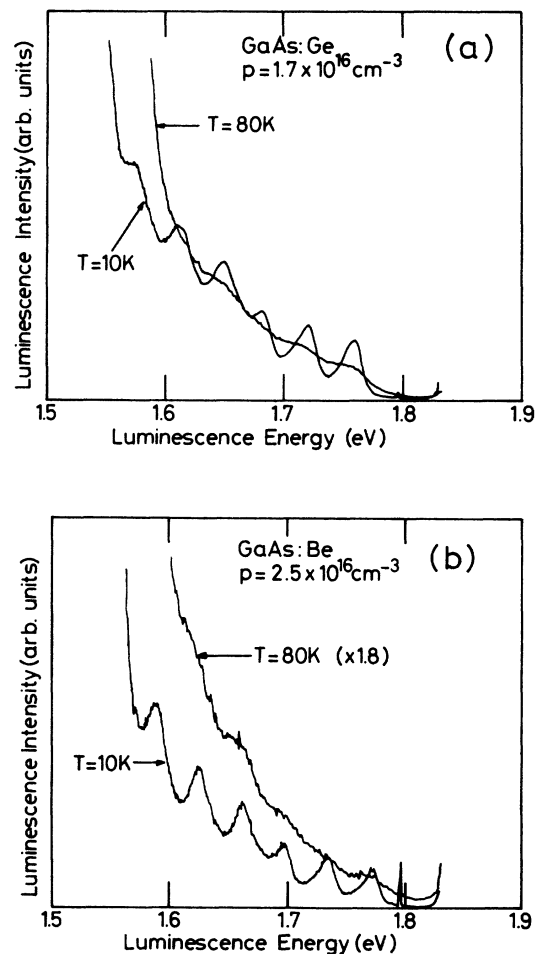


FIG. 14. (a) Hot-electron luminescence spectra for  $T=10$  K and for  $T=80$  K for Ge-doped GaAs. (b) Temperature dependence of hot-electron luminescence spectra for Be-doped GaAs.

broadening of the luminescence peaks implies that either additional scattering mechanisms appear, or that existing scattering mechanisms get stronger at these higher temperatures. There are two candidates for increased scattering. One is piezoelectric scattering by acoustic phonons which is known to dominate in III-V compound semiconductors in this temperature range. A different possibility is the increase of electron-electron scattering and electron-hole scattering due to the reduced screening at higher temperatures. We are presently investigating the effects of these additional scattering mechanisms.

Determination of the temperature dependence of the cw hot-electron luminescence spectra yields information on the temperature dependence of the various scattering channels open to electrons high in the conduction band.

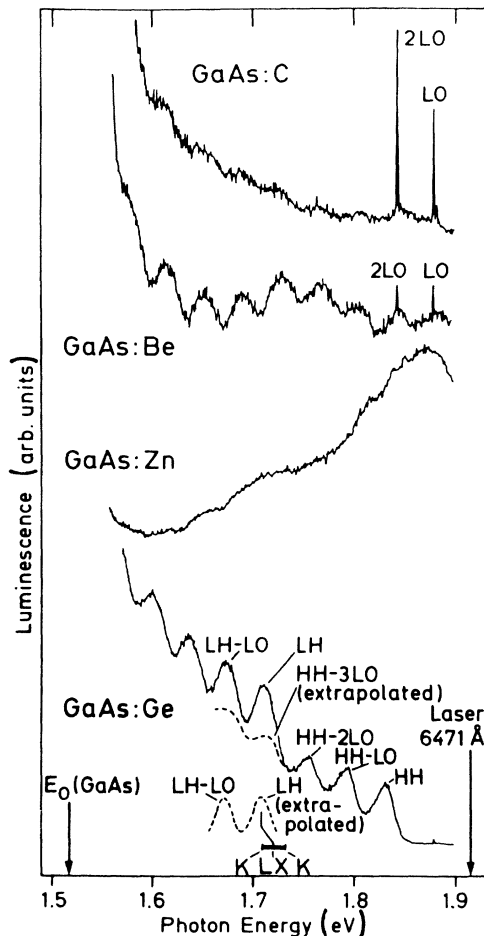


FIG. 15. This figure shows that for higher laser energies there is a dramatic dependence of the hot-electron luminescence spectra on the type of doping. This result indicates that the luminescence involves levels at higher-conduction- or valence-band extrema. Note that for low dye-laser energies hot-electron spectra show almost no dependence on dye-laser energy (apart from the shift according to difference in acceptor binding energy).

#### X. DEPENDENCE ON THE TYPE OF ACCEPTOR FOR DYE-LASER ENERGIES ABOVE 1.8 eV

Figures 2 and 3 show that the luminescence spectra from the hot-electron cascade are very similar for different types of acceptors (C, Be, Zn, and Ge) as long as the dye-laser energies remain below 1.9 eV. We showed that the spectra are shifted by the difference of the acceptor binding energies, while the shapes remain exactly the same apart from this uniform shift in energy position. In the dye-laser energy region between around 1.9 and 2.0 eV the spectra depend very strongly on the type of acceptor. Figure 15 shows the hot-electron luminescence spectra for GaAs:Ge, GaAs:Zn, GaAs:Be, and GaAs:C samples excited by the 6471 Å (= 1.916 eV) krypton-ion-laser line. The different samples show dramatically different hot-electron luminescence spectra, depending on the type of acceptor. Figures 16 and 17 explore the excitation energy range 1.85–2.01 eV further for GaAs:Be and for GaAs:C, while the spectra for GaAs:Ge were shown in Fig. 4. As a new feature a strong and broad peak appears, which peaks around 1.9 eV. Olego and Cardona<sup>31</sup> have investigated this type of luminescence in detail and have associated it with acceptor states at the split-off valence band, hence the dependence of these spectra on the type of acceptor. Thus this type of luminescence shows a component below  $E_0 + \Delta_0$  associated with transitions involving an acceptor, plus a component associated with direct transitions of holes in the split-off valence band.

Measurements at still higher excitation energies are shown in Fig. 18. At this higher excitation energy, the

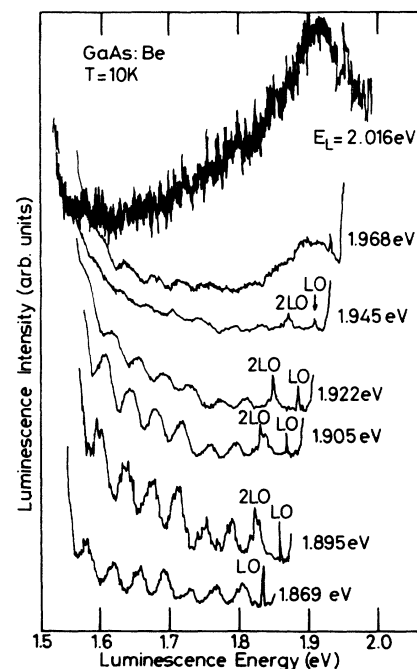


FIG. 16. Hot-electron luminescence spectra of Be-doped *p*-type GaAs for a series of dye-laser energies.

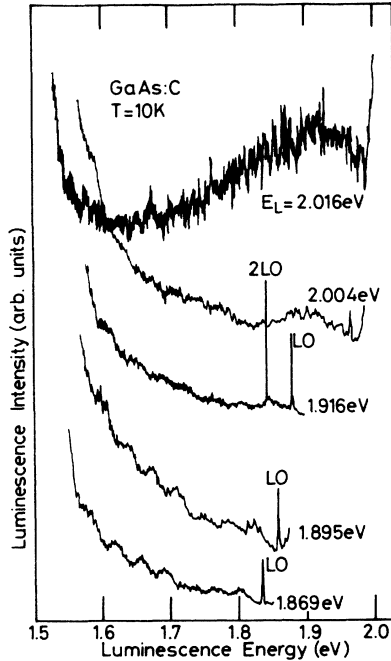


FIG. 17. Hot-electron luminescence spectra of C-doped  $p$ -type GaAs for a series of dye-laser energies.

spectra become virtually independent of the type of acceptor again: a hot-electron cascade below around 1.8 eV is found, which is caused by electrons relaxing in the  $\Gamma$  valley by emission of LO phonons, after returning from the  $L$  conduction-band valley. As the energy position of this cascade depends only on the energy position of the minimum of the  $L$  valley with respect to the  $\Gamma$  conduction-band valley, this luminescence is independent of the exciting laser energy. This effect has been previously studied in detail.<sup>2,14,31</sup>

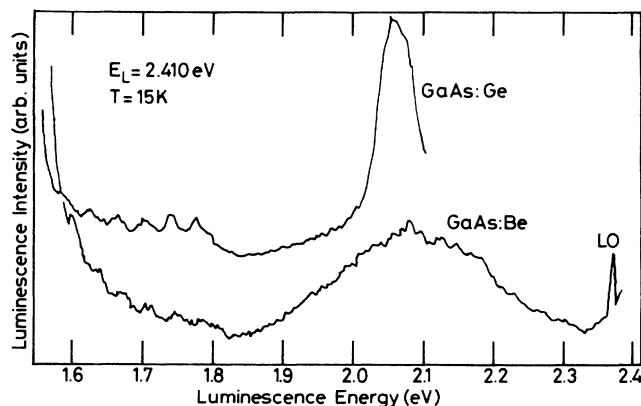


FIG. 18. Hot-electron luminescence spectrum excited with a laser energy of 2.41 eV. At this energy electrons are transferred in large amounts to the  $L$  and the  $X$  valleys. Reentrant spectra can be seen below 1.8 eV.

## XI. LUMINESCENCE FROM A DEEP DONOR AT POINTS $X$ OR $L$

In Fig. 4 the hot-electron luminescence spectrum of GaAs:Ge showed a peak at 1.738 eV for dye-laser energies in the range 1.95–1.99 eV. This peak is marked by an asterisk in Fig. 4 and it is shown in detail in Fig. 19. Figure 4 shows that this peak does not depend on the dye-laser energy, contrary to the luminescence peaks from the hot-electron cascade. This fact implies that the signal must come from a transition between two levels which are independent of  $k$ . Our interpretation is, that the transition observed here is due to a transition from a donor state associated with a higher conduction-band minimum. We cannot at this stage determine whether the relevant conduction-band minimum is point  $X$  or  $L$ . Comparison with Figs. 16 and 17 show that this peak is absent in samples where the acceptors are carbon or beryllium. This finding is consistent with our explanation, since germanium is the only impurity considered here which can be incorporated into GaAs as an acceptor or as a donor. In the MBE growth process the substrate temperature determines whether the germanium impurities occupy predominantly acceptor or donor positions. Thus by the choice of the substrate temperature, MBE-grown GaAs can be made  $p$  type or  $n$  type depending on the substrate temperature. This technique has been studied in detail by Künzel *et al.*<sup>32</sup> Thus we conclude that the observed transition is due to a transition between an electron trapped in germanium donor level at point  $X$  or  $L$  with a hole on a neutral germanium acceptor. In the case of the donor being at point  $X$ , using  $E(\Gamma_8-X_6) = 2.010 \pm 0.008$  eV,<sup>33</sup> the binding energy would be  $E_x^* = 231 \text{ meV} \pm 10 \text{ meV} + \langle E_C \rangle$ .  $\langle E_C \rangle$  is the Coulomb energy, i.e., the difference between the peak energy of the donor-acceptor-pair luminescence band and  $E_g - E_A - E_d$  due to the Coulomb interaction between the ionized donor and the ionized acceptor after the luminescence transition has taken place.  $\langle E_C \rangle$  is of the order of 30 meV.<sup>34</sup> In case the relevant transition is between a donor level at point  $X$  and the acceptor,  $E_x^*$  is therefore close to 260 meV, which is comparable to the binding energy of Ge at the  $X$  point in GaP,<sup>35,36</sup> which is 201.5 meV. In the case that the observed signal is due to a donor associated with  $L$ , the binding energy would be  $E_L^* = 58 \pm 5 \text{ meV} + \langle E_C \rangle$ , where we are using  $E(\Gamma_6-L_6) = 320 \pm 4$  eV.<sup>14</sup> At this stage we cannot unambiguously determine whether transitions involve donor levels at points  $X$  or  $L$ , but pressure measurements should be able to determine the precise nature of the donor level, as the pressure coefficients of the  $X$  and  $L$  conduction bands are very different.

Note that the luminescence signal at 1.738 eV only appears for dye-laser energies in a very narrow energy range, 1.95 to 1.99 eV. We could not detect this particular luminescence peak at any other dye-laser energy. Within this narrow dye-laser energy range, on the other hand, the luminescence peak at 1.738 eV dominates the total hot-electron spectrum, as Fig. 19 demonstrates. Thus it is indicated that a resonant excitation process occurs. This resonance also appears as a strong dip in



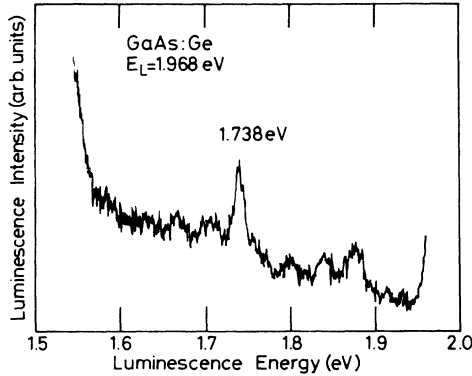


FIG. 19. Hot-electron luminescence spectrum of Ge-doped GaAs, showing evidence of a line at 1.783 eV, which we assign to recombination between an electron at a deep donor level at point  $X$  or  $L$  with a neutral acceptor.

the measurement of the ordinary hot-electron luminescence spectrum as a function of dye-laser energy (Fig. 5 in Ref. 7). We conclude that for dye-laser energies in the range 1.95–1.99 eV, excitation of electrons is into a resonant state, most probably into a germanium donor state composed of  $X$  or  $L$  wave functions. It is quite possible that this donor state is resonant with the conduction band, leading to predominant laser excitation into this localized state. This luminescence method allows the study of donor states at higher conduction-band minima.

## XII. SUMMARY

We have investigated in detail the luminescence from the steady-state distribution of laser-excited electrons in the conduction band of GaAs relaxing by emission of LO phonons. This luminescence contains a wealth of information on ultrafast scattering processes taking place on a time scale of 100 fs. We extract information on the band structure of GaAs in approximately the first tenth of the Brillouin zone around point  $\Gamma$ . Band-structure information is obtained by determining the dependence of the hot-electron luminescence spectra on the dye-laser energy. This technique is equivalent and complementary to energy-resolved photoemission experiments from negative affinity coated GaAs, except that the energy resolution of the cw hot-electron luminescence experiments is higher.

Using a  $16 \times 16$   $\mathbf{k} \cdot \mathbf{p}$  band-structure calculation and determining the optical transition-matrix elements in the dipole model we calculate the transient distribution of electrons in the conduction band and the expected theoretical luminescence line shapes. The experimental line shapes are considerably broadened with respect to the theoretical line shapes. We determine the details of the broadening and deduce the LO-phonon scattering times, and the  $\Gamma \rightarrow L$  scattering times, and their dependence on the electron kinetic energy. This determination is only weakly dependent on the relative lack of information on the composition of the acceptor wave functions

and the conduction band to acceptor matrix elements, as a function of  $\mathbf{k}$ . An alternative way of determining the scattering times is from the intensities of the hot-electron luminescence peaks. Indeed, measuring the hot-electron cascade as a function of dye-laser energy for different acceptors will yield information on the composition of the acceptor wave functions.

For the LO-phonon scattering time we determine  $\tau_{LO} = 132 \pm 10$  fs, while for the  $\Gamma \rightarrow L$  scattering time  $\tau_{\Gamma \rightarrow L}$  we find values between 100 and 200 fs depending on the electron kinetic energy. For the associated deformation potential we determine  $D_{\Gamma \rightarrow L} = (9.5 \pm 1.6) \times 10^8$  eV/cm. These two scattering times are of tremendous importance both for fundamental reasons as well as technological ones, as they are needed in Monte Carlo simulations of transistors including superfast hot-electron transistors. The  $\Gamma \rightarrow L$  scattering time  $\tau_{\Gamma \rightarrow L}$  also determines the saturation velocity. The importance of the present technique is that it avoids many of the problems associated with the more common femtosecond pulsed laser techniques, which have lower sensitivity and lower spectral resolution (Heisenberg's uncertainty relationship limits the spectral resolution of ultrashort laser pulses). Most important of all, ultrashort laser pulses always severely disturb the sample due to the very high light density, and due to a pulsed heating effect. Ultrashort laser pulse experiments therefore always are under conditions of very high nonequilibrium carrier concentration. The present experiments study the electron relaxation processes under low carrier density, and in addition they also allow studies at higher densities as well. Thus we gain the possibility of studying the carrier relaxation as a function of carrier concentration. Such experiments are in progress in our laboratory.

In addition to the determination of these scattering times, there is a variety of other information contained in the cw hot-electron luminescence experiments. Thus we have obtained information on Ge donor levels at higher-conduction-band minima.

## ACKNOWLEDGMENTS

The help and support of this work by M. Cardona are gratefully acknowledged. One of us (G.F.) gratefully acknowledges helpful discussions with P. Lugli, J. Shah, K. Ploog, R. G. Ulbrich, and J. C. Tsang, and many discussions and support from H. Sakaki. This work was partially supported by the Science and Engineering Research Council (SERC) of United Kingdom, the Max-Planck-Institute für Festkörperforschung, Stuttgart, Germany and the Institute for Physical and Chemical Research (RIKEN), Wako-shi, Saitama-ken, Japan. Part of this work was performed at the Max-Planck-Institut für Festkörperforschung, Heisenbergstrasse 1, D-7000 Stuttgart 80, West Germany, the Institute of Industrial Science, University of Tokyo, 7-22-1 Roppongi, Minatoku, Tokyo 106, Japan, and the Research Center for Advanced Science and Technology (RCAT), University of Tokyo, 4-6-1 Komaba, Meguro-ku, Tokyo 153, Japan.

- \*Present address: Sakaki Quantum Wave Project, Exploratory Research for Advanced Technology (ERATO) Program of the Science and Technology Agency, Keyaki House 302, 4-3-24 Komaba, Meguro-ku, Tokyo 153, Japan.
- <sup>1</sup>Jagdeep Shah and R. C. C. Leite, *Phys. Rev. Lett.* **22**, 1304 (1969).
- <sup>2</sup>B. P. Zakharchenya, V. D. Dymnikov, I. Ya. Karlik, and I. I. Reshina, *J. Phys. Soc. Jpn.* **49**, 573 (1980); B. P. Zakharchenya, D. N. Mirlin, V. I. Perel, and I. I. Reshina, *Usp. Fiz. Nauk* **136**, 459 (1982) [*Sov. Phys. Usp.* **25**, 143 (1982)], and references therein.
- <sup>3</sup>D. N. Mirlin, I. Ya. Karlik, L. P. Nikitin, I. I. Reshina, and V. F. Sapega, *Solid State Commun.* **37**, 757 (1981).
- <sup>4</sup>S. A. Lyon and C. L. Petersen, *Ultrafast Laser Probe Phenomena in Bulk and Microstructure Semiconductors II* [*Proc. SPIE* **942**, 264 (1988)].
- <sup>5</sup>M. A. Alekseev, I. Ya. Karlik, D. N. Mirlin, and V. F. Sapega, *Fiz. Tekh. Poluprovodn.* **22**, 569 (1988) [*Sov. Phys.—Semicond.* **22**, 355 (1988)].
- <sup>6</sup>G. Fasol, K. Ploog, and E. Bauser, *Solid State Commun.* **54**, 383 (1985).
- <sup>7</sup>G. Fasol and H. P. Hughes, Title, *IOP Conf. Proc. Ser. No. 79*, edited by M. Fujimoto (Hilger, Bristol, 1986), p. 253.
- <sup>8</sup>G. Fasol and H. P. Hughes, *Phys. Rev. B* **33**, 2953 (1986).
- <sup>9</sup>H.-J. Drouhin, C. Hermann, and G. Lampel, *Phys. Rev. B* **31**, 3859 (1985).
- <sup>10</sup>H.-J. Drouhin, C. Hermann, and G. Lampel, *Phys. Rev. B* **31**, 3872 (1985).
- <sup>11</sup>R. G. Ulbrich, J. A. Kash, and J. C. Tsang, *Phys. Rev. Lett.* **62**, 949 (1989).
- <sup>12</sup>R. G. Ulbrich, *Solid State Electron.* **21**, 51 (1978).
- <sup>13</sup>D. Olego and M. Cardona, *Phys. Rev. B* **22**, 886 (1980); **22**, 1905 (1980).
- <sup>14</sup>E. A. Imhoff, M. I. Bell, and R. A. Forman, *Solid State Commun.* **54**, 845 (1985).
- <sup>15</sup>R. W. Shaw, *Phys. Rev. B* **10**, 3283 (1971).
- <sup>16</sup>R. G. Ulbrich, *Phys. Rev. Lett.* **27**, 1512 (1971).
- <sup>17</sup>U. Rössler, *Solid State Commun.* **49**, 943 (1984).
- <sup>18</sup>M. Cardona, N. E. Christensen, and G. Fasol, *Phys. Rev. B* **38**, 1806 (1988).
- <sup>19</sup>H.-J. Drouhin, C. Hermann, and G. Lampel, *Phys. Rev. B* **31**, 3859 (1985).
- <sup>20</sup>H.-J. Drouhin, C. Hermann, and G. Lampel, *Phys. Rev. B* **31**, 3872 (1985).
- <sup>21</sup>P. B. Allen, *Phys. Status Solidi B* **120**, 529 (1983).
- <sup>22</sup>M. Cardona, N. E. Christensen, and G. Fasol, *Phys. Rev. Lett.* **56**, 2831 (1986).
- <sup>23</sup>J. A. Kash, J. C. Tsang, and J. Hvam, *Phys. Rev. Lett.* **54**, 2151 (1985).
- <sup>24</sup>A. F. J. Levi, J. R. Hayes, P. M. Platzman, and W. Wiegmann, *Phys. Rev. Lett.* **55**, 2071 (1985).
- <sup>25</sup>J. Shah, B. Devaud, T. Damen, W. Tsang, A. Gossard, and P. Lugli, *Phys. Rev. Lett.* **59**, 2222 (1987).
- <sup>26</sup>C. Collins and P. Yu, *Phys. Rev. B* **30**, 4501 (1984).
- <sup>27</sup>R. G. Ulbrich (private communication).
- <sup>28</sup>P. J. Dean, D. D. Manchon, and J. J. Hopfield, *Phys. Rev. Lett.* **25**, 1027 (1970).
- <sup>29</sup>A. S. Barker, *Phys. Rev.* **7**, 2507 (1973).
- <sup>30</sup>D. J. Ashen, P. J. Dean, D. T. J. Hurle, J. B. Mullin, A. M. White, and P. D. Greene, *J. Phys. Chem. Solids* **36**, 1041 (1975).
- <sup>31</sup>D. Olego and M. Cardona, *Phys. Rev. B* **22**, 1905 (1980).
- <sup>32</sup>H. Künzel, A. Fischer, and K. Ploog, *Appl. Phys.* **22**, 23 (1980).
- <sup>33</sup>D. J. Wolford and J. A. Bradley, *Solid State Commun.* **53**, 1069 (1985).
- <sup>34</sup>D. G. Thomas, M. Gershenzon, and F. A. Trumbore, *Phys. Rev.* **133**, A269 (1964).
- <sup>35</sup>M. Altarelli, *J. Phys. Soc. Jpn., Suppl. A* **49**, 169 (1980).
- <sup>36</sup>A. T. Vink, R. L. A. Van der Heyden, and J. A. W. Van der Does de Bye, *J. Lumin.* **8**, 105 (1973).
- <sup>37</sup>W. Fawcett, A. Boardman, and S. Swain, *J. Phys. Chem. Solids* **31**, 1963 (1970).
- <sup>38</sup>K. Kash, P. Wolff, and W. Bonner, *Appl. Phys. Lett.* **42**, 173 (1983).

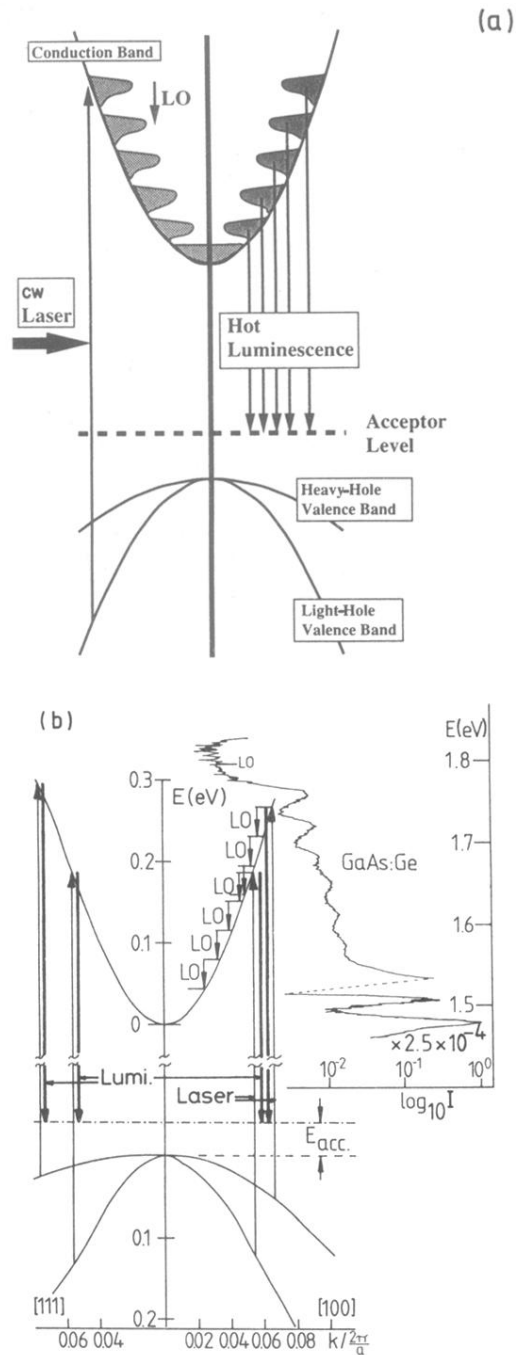


FIG. 1. (a) Schematic of cw spectroscopy of ultrafast processes in GaAs. The vertical arrow on the left shows excitation of electrons from the light-hole valence band to the conduction band by a cw dye laser. The steady-state distribution of electrons consists of a series of peaks, spaced by the LO-phonon energy. Individual electrons take only a few hundred femtoseconds to relax through this cascade. The luminescence transitions are indicated as vertical arrows. For clarity only processes involving the light-hole band are shown in (a). In the experiment, equivalent processes involving the heavy-hole band are superimposed. (b) This figure shows hot-electron luminescence near point  $\Gamma$  to scale. The steady-state distribution of electrons excited both from the heavy- and the light-hole bands are shown to scale. The inset on the right-hand side shows the corresponding luminescence spectrum on a logarithmic scale.